

Gated Recurrent Neural Networks with Weighted Time-Delay Feedback

N. Benjamin Erichson*

University of Pittsburgh
and ICSI

erichson@icsi.berkeley.edu

Soon Hoe Lim*

Nordita, KTH Royal Institute of Technology
and Stockholm University

soon.hoe.lim@su.se

Michael W. Mahoney

ICSI, LBNL, and UC Berkeley

mmahoney@stat.berkeley.edu

Abstract

We introduce a novel gated recurrent unit (GRU) with a weighted time-delay feedback mechanism in order to improve the modeling of long-term dependencies in sequential data. This model is a discretized version of a continuous-time formulation of a recurrent unit, where the dynamics are governed by delay differential equations (DDEs). By considering a suitable time-discretization scheme, we propose τ -GRU, a discrete-time gated recurrent unit with delay. We prove the existence and uniqueness of solutions for the continuous-time model, and we demonstrate that the proposed feedback mechanism can help improve the modeling of long-term dependencies. Our empirical results show that τ -GRU can converge faster and generalize better than state-of-the-art recurrent units and gated recurrent architectures on a range of tasks, including time-series classification, human activity recognition, and speech recognition.

1 Introduction

Recurrent neural networks (RNNs) and their variants are flexible gradient-based methods specially designed to model sequential data. Models of this type can be viewed as dynamical systems whose temporal evolution is governed by a system of differential equations driven by an external input. Indeed, there is a long-standing tradition to formulate continuous-time variants of RNNs [50]. In this setting, the data are formulated in continuous-time, i.e., inputs are defined by the function $\mathbf{x} = \mathbf{x}(t) \in \mathbb{R}^p$ and targets are defined as $\mathbf{y} = \mathbf{y}(t) \in \mathbb{R}^q$. In this way, one can, for instance, employ a nonautonomous ordinary differential equation (ODE) to model the dynamics of the hidden states $\mathbf{h}(t) \in \mathbb{R}^d$, where t denotes continuous time, as

$$\frac{d\mathbf{h}(t)}{dt} = f(\mathbf{h}(t), \mathbf{x}(t); \boldsymbol{\theta}).$$

Here, $f : \mathbb{R}^d \times \mathbb{R}^p \rightarrow \mathbb{R}^d$ is a function which is parameterized by a neural network (NN) with the learnable weights $\boldsymbol{\theta}$. A prototypical choice for f is the tanh recurrent unit:

$$f(\mathbf{h}(t), \mathbf{x}(t); \boldsymbol{\theta}) := \tanh(\mathbf{W}\mathbf{h}(t) + \mathbf{U}\mathbf{x}(t) + \mathbf{b}),$$

where $\mathbf{W} \in \mathbb{R}^{d \times d}$ denotes a hidden-to-hidden weight matrix, $\mathbf{U} \in \mathbb{R}^{d \times p}$ an input-to-hidden weight matrix, and \mathbf{b} a bias term. With this continuous-time formulation in hand, one can then use tools from dynamical systems theory to study the dynamical behavior of the model as well as to motivate mechanisms that can prevent rapidly diverging or converging dynamics. For instance, [11] proposed a parametrization of the hidden-to-hidden matrix as an antisymmetric matrix to ensure stable hidden state dynamics, and [15] relaxed this idea to improve model expressivity. More recently, [53] has proposed an RNN architecture based on a suitable time-discretization of a set of coupled multiscale ODEs.

*Equal contribution.

τ -GRU

Continuous-time formulation of τ -GRU:

$$\frac{d\mathbf{h}(t)}{dt} = \underbrace{u(\mathbf{h}(t), \mathbf{x}(t))}_{\text{instantaneous dynamics}} + \underbrace{a(\mathbf{h}(t), \mathbf{x}(t)) \odot z(\mathbf{h}(t - \tau), \mathbf{x}(t))}_{\text{weighted time-delayed feedback}} - \mathbf{h}(t) \quad (1)$$

Discrete-time formulation of τ -GRU:

$$\mathbf{h}_{n+1} = (1 - \mathbf{g}_n) \odot \mathbf{h}_n + \mathbf{g}_n \odot (\mathbf{u}_n + \mathbf{a}_n \odot \mathbf{z}_n) \quad (2)$$

with

$$\mathbf{u}_n = u(\mathbf{h}_n, \mathbf{x}_n) := \tanh(\mathbf{W}_1 \mathbf{h}_n + \mathbf{U}_1 \mathbf{x}_n) \quad (3)$$

$$\mathbf{z}_n = z(\mathbf{h}_n, \mathbf{x}_n) := \tanh(\mathbf{W}_2 \mathbf{h}_n + \mathbf{U}_2 \mathbf{x}_n) \quad (4)$$

$$\mathbf{g}_n = g(\mathbf{h}_n, \mathbf{x}_n) := \text{sigmoid}(\mathbf{W}_3 \mathbf{h}_n + \mathbf{U}_3 \mathbf{x}_n) \quad (5)$$

$$\mathbf{a}_n = a(\mathbf{h}_n, \mathbf{x}_n) := \text{sigmoid}(\mathbf{W}_4 \mathbf{h}_n + \mathbf{U}_4 \mathbf{x}_n) \quad (6)$$

input	\mathbf{x}	\mathbb{R}^p
time index	t	\mathbb{R}
time delay	τ	\mathbb{R}
hidden state	\mathbf{h}	\mathbb{R}^d
hidden-to-hidden matrix	\mathbf{W}_i	$\mathbb{R}^{d \times d}$
input-to-hidden matrix	\mathbf{U}_i	$\mathbb{R}^{d \times p}$
decoder matrix	\mathbf{V}	$\mathbb{R}^{q \times d}$

$$\mathbf{h}_n \approx \mathbf{h}(t_n), t_n = n\Delta t, n = 0, 1, \dots$$

$$l := n - \lfloor \tau / \Delta t \rfloor$$

In this work, we consider using input-driven delay differential equations (DDEs) to model the dynamics of the hidden states:

$$\frac{d\mathbf{h}(t)}{dt} = f(\mathbf{h}(t), \mathbf{h}(t - \tau), \mathbf{x}(t); \boldsymbol{\theta}),$$

where τ is a constant that indicates the delay (i.e., time-lag). Here, the time derivative is described by a function $f : \mathbb{R}^d \times \mathbb{R}^d \times \mathbb{R}^p \rightarrow \mathbb{R}^d$ that explicitly depends on states from the past. In prior work [43], it has been shown that delay units can greatly improve performance on long-term dependency problems [48], i.e., problems for which the desired model output depends on inputs presented at times far in the past.

In more detail, we propose a novel continuous-time recurrent unit, given in Eq. (1), that is composed of two parts: (i) a component $u(\mathbf{h}(t), \mathbf{x}(t))$ that explicitly models instantaneous dynamics; and (ii) a component $z(\mathbf{h}(t - \tau), \mathbf{x}(t))$ that provides time-delayed feedback to account for non-instantaneous dynamics. The feedback also helps to propagate gradient information more efficiently, thus lessening the issue of vanishing gradients. In addition, we introduce $a(\mathbf{h}(t), \mathbf{x}(t))$ to weight the importance of the feedback component-wise, which helps to better model different time scales. By considering a suitable time-discretization scheme of this continuous-time setup, we obtain a gated recurrent unit (GRU), given in Eq. (2), which we call τ -GRU. The individual parts are described by Eq. (3)-(6), where \mathbf{g}_n and \mathbf{a}_n resemble commonly used gating functions.

Main Contributions. Here are our main contributions.

- **Design.** We introduce a novel gated recurrent unit, which we call τ -GRU, that incorporates a weighted time-delay feedback mechanism to lessen the vanishing gradients issue. This model is motivated by DDEs, and it is obtained by discretizing the continuous Eq. (1).
- **Theory.** We show that the continuous-time τ -GRU model has a unique well-defined solution (see Theorem 1). Moreover, we provide intuition and analysis to understand how the introduction of delays in τ -GRU can act as a buffer to help lessen the vanishing gradients problem, thus improving the ability to retain information far in the past. See Proposition 1 for a simplified setting and Proposition 3 for τ -GRU.
- **Experiments.** We provide empirical results to demonstrate the superior performance of τ -GRU, when compared to other RNN architectures, on a variety of benchmark tasks. In particular, we show that τ -GRU converges faster during training and can achieve improved generalization performance. Moreover, we demonstrate that it provides favorable trade-offs between effectiveness in dealing with long-term dependencies and expressivity in the considered tasks. See Figure 1 for an illustration of this.

2 Related Work

Here, we discuss recent RNN advances that have been demonstrated to outperform classic architectures such as Long Short Term Memory (LSTM) networks [24] and Gated Recurrent Units (GRUs) [13]. We also

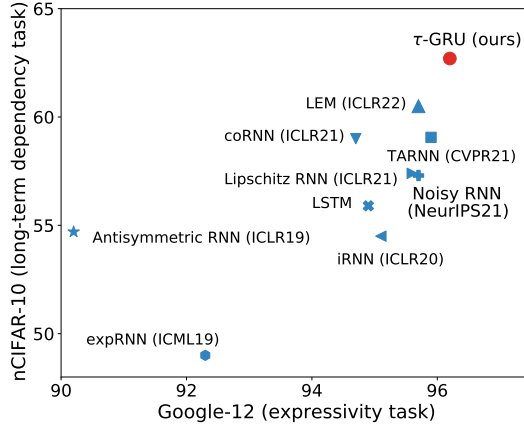


Figure 1: Test accuracy for nCIFAR [11] versus Google-12 [61]. nCIFAR requires a recurrent unit with long-term dependency capabilities, while Google-12 requires a highly expressive unit. Our proposed τ -GRU is able to improve performance on both tasks, relative to existing state-of-the-art alternatives, including LEM [53].

briefly discuss prior works on incorporating delays into neural architectures. (We omit a detailed discussion of other recent deep learning models for sequential problems that leverage dynamical system theory: [17, 5, 20, 56, 23].)

Unitary and orthogonal RNN. The seminal work by [2] introduced a recurrent unit where the hidden weight matrix is constructed as the product of unitary matrices. This enforces that the eigenvalues lie on the unit circle. This, in turn, prevents vanishing and exploding gradients, thereby enabling the learning of long-term dependencies. However, such unitary RNNs suffer from limited expressivity, since the construction of the hidden matrix is restrictive [4]. Work by [62] and [59] partially addressed this issue by considering the Cayley transform on skew-symmetric matrices; and work by [39, 38] leveraged skew-Hermitian matrices to parameterize the orthogonal group to improve expressiveness. The expressiveness of RNNs has been further improved by considering nonnormal hidden matrices [29].

Continuous-time RNNs. The recent work on Neural ODEs [12] and variants [30, 51, 63, 22] have motivated the formulation of several modern continuous-time RNNs, which are expressive and have good long-term memory. The work by [11] used an antisymmetric matrix to parameterize the hidden-to-hidden matrix in order to obtain stable dynamics. This was later relaxed by [15]. In [27], a modified differential equation was considered, which allows one to update the hidden states based on the difference between predicted and previous states. Work by [52] demonstrated that long-term memory can be improved by modeling the hidden dynamics by a second-order system of ODEs, which models a coupled network of controlled forced and damped nonlinear oscillators. Another approach for improving long-term memory was motivated by a time-adaptive discretization of an ODE [26]. The expressiveness of continuous-time RNNs has been further improved by introducing a suitable time-discretization of a set of multiscale ODEs [53]. It has also been shown that noise-injected RNNs can be viewed as discretizations of stochastic differential equations driven by input data [41]. In this case, the noise can help to stabilize the hidden dynamics during training and improve robustness to input perturbations.

Using delays in NNs. The idea of introducing delays into NNs goes back to [60, 34], where a time-delay NN was proposed to tackle the phoneme recognition problem. Several works followed: [31] considered a time-delayed RNN model that is suitable for temporal correlations and prediction of chaotic and financial time series; and delays were also incorporated into and studied within the nonlinear autoregressive with exogenous inputs (NARX) RNNs [43]. More recently, [66] introduced delay terms in Neural ODEs and demonstrated their outstanding approximation capacities. In particular, the model of [66] is able to learn delayed dynamics where the trajectories in the lower-dimensional phase space could be mutually intersected, while the Neural ODEs [12] are not able to do so.

3 Method

In this section, we first provide an introduction to DDEs; then, we motivate the formulation of our DDE-based models, in continuous as well as discrete time; and, finally, we propose a weighted time-delay feedback architecture.

Notation. \odot denotes Hadamard product, $|v|$ denotes vector norm for the vector v , $\|A\|$ denotes operator norm for the matrix A , σ and $\hat{\sigma}$ (or sigmoid) denote the tanh and sigmoid function, respectively; and $\lceil x \rceil$ and $\lfloor x \rfloor$ denote the ceiling function and floor function in x , respectively.

3.1 Background on Delay Differential Equations

DDEs are an important class of dynamical systems that arise in natural and engineering sciences [55, 18, 28]. In these systems, a feedback term is introduced to adjust the system non-instantaneously, resulting in delays in time. In mathematical terms, the derivative of the system state depends explicitly on the past value of the state variable.

Here, we focus on DDEs with a single discrete delay

$$\dot{h} = F(t, h(t), h(t - \tau)), \quad (7)$$

with $\tau > 0$, where F is a continuous function. Due to the presence of the delay term, we need to *specify an initial function* which describes the behavior of the system prior to the initial time 0. For the DDE, it would be a function ϕ defined on $[-\tau, 0]$. Hence, a DDE numerical solver must save all the information needed to approximate delayed terms.

Instead of thinking the solution of the DDE as consisting of a sequence of values of h at increasing values of t , as one would do for ODEs, it is more fruitful to view it as a mapping of functions on the interval $[t - \tau, t]$ into functions on the interval $[t, t + \tau]$, i.e., as a sequence of functions defined over a set of contiguous time intervals of length τ . Since the state of the system at time $t \geq 0$ must contain all the information necessary to determine the solution for future times $s \geq t$, it should contain the initial condition ϕ .

More precisely, the DDE is a functional differential equation with the state space $C := C([-\tau, 0], \mathbb{R}^d)$. This state space is the Banach space of continuous functions from $[-\tau, 0]$ into \mathbb{R}^d , with the topology of uniform convergence. It is equipped with the norm $\|\phi\| := \sup\{|\phi(\theta)| : \theta \in [-\tau, 0]\}$. In contrast to the ODEs (with $\tau = 0$) whose state space is finite-dimensional, DDEs are generally infinite-dimensional dynamical systems. Various aspects of DDEs have been studied, including their solution properties [21, 3], dynamics [37, 6] and stability [46, 8, 40, 64, 47].

3.2 Formulation of Continuous-Time τ -GRUs

The basic form of a time-delayed RNN is

$$\dot{\mathbf{h}} = \sigma(\mathbf{W}_1 \mathbf{h}(t) + \mathbf{W}_2 \mathbf{h}(t - \tau) + \mathbf{U} \mathbf{x}(t)) - \mathbf{h}(t), \quad (8)$$

for $t \geq 0$, and $\mathbf{h}(t) = \mathbf{0}$ for $t \in [-\tau, 0]$, with the output $\mathbf{y}(t) = \mathbf{V} \mathbf{h}(t)$. In this expression, $\mathbf{h} \in \mathbb{R}^d$ denotes the hidden states, $f : \mathbb{R}^d \times \mathbb{R}^d \times \mathbb{R}^p \rightarrow \mathbb{R}^d$ is a nonlinear function, and $\sigma : \mathbb{R} \rightarrow (-1, 1)$ denotes the tanh activation function applied component-wise. The matrices $\mathbf{W}_1, \mathbf{W}_2 \in \mathbb{R}^{d \times d}$, $\mathbf{U} \in \mathbb{R}^{d \times p}$ and $\mathbf{V} \in \mathbb{R}^{q \times d}$ are learnable parameters, and $\tau \geq 0$ denotes the discrete time-lag. For notational brevity, we omit the bias term here, assuming it is included in \mathbf{W}_1 .

It is important to equip RNNs with mechanism to better represent a large number of scales, as discussed by [57] and more recently by [53]. Therefore, we follow [57] and consider a time warping function $c : \mathbb{R}^d \rightarrow \mathbb{R}^d$ which we define to be a parametric function $c(t)$. Using the reasoning in [57], and denoting $t_\tau := t - \tau$, we can formulate the following continuous-time delay recurrent unit

$$\dot{\mathbf{h}} = \frac{dc(t)}{dt} [\sigma(\mathbf{W}_1 \mathbf{h}(t) + \mathbf{W}_2 \mathbf{h}(t_\tau) + \mathbf{U}_1 \mathbf{x}(t)) - \mathbf{h}(t)].$$

Now, we need a learnable function to model $\frac{dc(t)}{dt}$. A natural choice is to consider a standard gating function, which is a universal approximator, taking the form

$$\frac{dc(t)}{dt} = \hat{\sigma}(\mathbf{W}_3 \mathbf{h}_t + \mathbf{U}_3 \mathbf{x}_t) =: \mathbf{g}(t), \quad (9)$$

where $\mathbf{W}_3 \in \mathbb{R}^{d \times d}$ and $\mathbf{U}_3 \in \mathbb{R}^{d \times p}$ are learnable parameters, and where $\hat{\sigma} : \mathbb{R} \rightarrow (0, 1)$ is the component-wise sigmoid function.

3.3 From Continuous to Discrete-Time τ -GRUs

To learn the weights of the recurrent unit, a numerical integration scheme can be used to discretize the continuous model. Specifically, we discretize the time as $t_n = n\Delta t$ for $n = -\lfloor \tau/\Delta t \rfloor, \dots, -1, 0, 1, \dots$, and approximate the solution $(\mathbf{h}(t))$ to Eq. (8) by the sequence $(\mathbf{h}_n = \mathbf{h}(t_n))$, given by $\mathbf{h}_n = 0$ for $n = -\lfloor \tau/\Delta t \rfloor, \dots, 0$, and

$$\mathbf{h}_{n+1} = \mathbf{h}_n + \int_{t_n}^{t_n+\Delta t} f(\mathbf{h}(s), \mathbf{h}(s-\tau), \mathbf{x}(s)) ds \quad (10)$$

$$\approx \mathbf{h}_n + \text{scheme}[f, \mathbf{h}_n, \mathbf{h}_l, \Delta t], \quad (11)$$

for $n = 0, 1, \dots$, where the subscript n denotes discrete time indices, $l := n - \lfloor \tau/\Delta t \rfloor$, and Δt represents the time difference between a pair of consecutive elements in the input sequence. In addition, `scheme` refers to a numerical integration scheme whose application yields an approximate solution for the integral. Using the explicit forward Euler scheme and choosing $\Delta t = 1$ gives:

$$\mathbf{h}_{n+1} = (1 - \mathbf{g}_n) \odot \mathbf{h}_n + \mathbf{g}_n \odot \sigma(\mathbf{W}_1 \mathbf{h}_n + \mathbf{W}_2 \mathbf{h}_l + \mathbf{U} \mathbf{x}_n). \quad (12)$$

Note that this discretization corresponds to the leaky-integrator described by [25].

It can be shown that (12) is a universal approximator of a large class of open dynamical systems with delay (see Theorem 4). However, the performance of this architecture is not able to outperform state-of-the-art RNN architectures on a number of tasks. To improve the performance, we propose a modified gated recurrent unit next.

3.4 Discrete-Time τ -GRUs with a Weighted Time-Delay Feedback Architecture

In this work, we propose to model the hidden dynamics using a mixture of a standard recurrent unit and a delay recurrent unit. To this end, we replace the σ in Eq. (12) by

$$\mathbf{u}_n + \mathbf{a}_n \odot \mathbf{z}_n, \quad (13)$$

so that we yield a new GRU that takes the form

$$\mathbf{h}_{n+1} = (1 - \mathbf{g}_n) \odot \mathbf{h}_n + \mathbf{g}_n \odot (\mathbf{u}_n + \mathbf{a}_n \odot \mathbf{z}_n). \quad (14)$$

Here \mathbf{u}_n describes the standard recurrent unit

$$\mathbf{u}_n = \tanh(\mathbf{W}_1 \mathbf{h}_n + \mathbf{U}_1 \mathbf{x}_n),$$

and \mathbf{z}_n describes the delay recurrent unit

$$\mathbf{z}_n = \tanh(\mathbf{W}_2 \mathbf{h}_l + \mathbf{U}_2 \mathbf{x}_n).$$

Further, the gate \mathbf{g}_n is a learnable vector-valued coefficient

$$\mathbf{g}_n = \text{sigmoid}(\mathbf{W}_3 \mathbf{h}_n + \mathbf{U}_3 \mathbf{x}_n).$$

The weighting term \mathbf{a}_n is also a vector-valued coefficient

$$\mathbf{a}_n = \text{sigmoid}(\mathbf{W}_4 \mathbf{h}_n + \mathbf{U}_4 \mathbf{x}_n),$$

with the learnable parameters $\mathbf{W}_4 \in \mathbb{R}^{d \times d}$ and $\mathbf{U}_4 \in \mathbb{R}^{d \times p}$ that weights the importance of the time-delay feedback component-wise for the task on hand. From the design point of view, Eq. (13) can be motivated by the sigmoidal coupling used in Hodgkin-Huxley type neural models (see Eq. (1)-(2) and Eq. (4) in [9]).

4 Theory

In this section, we define the notion of solution for DDEs and show that the continuous-time τ -GRU has a unique solution. Moreover, we provide intuition and analysis to understand how the delay mechanism can help improving long-term dependencies.

4.1 Existence and Uniqueness of Solution for Continuous-Time τ -GRUs

Since we must know $h(t + \theta)$, $\theta \in [-\tau, 0]$ in order to determine the solution of the DDE (7) for $s > t$, we call the state of the dynamical system at time t the element of C which we denote as h_t , defined as $h_t(\theta) := h(t + \theta)$ for $\theta \in [-\tau, 0]$. The trajectory of the solution can thus be viewed as the curve $t \rightarrow h_t$ in the state space C . In general, DDEs can be formulated as the following initial value problem (IVP) for the nonautonomous system [21]:

$$\dot{h}(t) = f(t, h_t), \quad t \geq t_0, \quad (15)$$

where $h_{t_0} = \phi \in C$ for some initial time $t_0 \in \mathbb{R}$, and $f : \mathbb{R} \times C \rightarrow \mathbb{R}^d$ is a given continuous function. The above equation describes a general type of systems, including ODEs ($\tau = 0$) and DDEs of the form $\dot{h}(t) = g(t, h(t), h(t - \tau))$ for some continuous function g .

We say that a function h is a solution of Eq. (15) on $[t_0 - \tau, t_0 + A]$ if there exists $t_0 \in \mathbb{R}$ and $A > 0$ such that $h \in C([t_0 - \tau, t_0 + A], \mathbb{R}^d)$, $(t, h_t) \in \mathbb{R} \times C$ and $h(t)$ satisfies Eq. (15) for $t \in [t_0, t_0 + A]$. It can be shown that (see, for instance, Lemma 1.1 in [21]) if $f(t, \phi)$ is continuous, then finding a solution of Eq. (15) is equivalent to solving the integral equation: $h_{t_0} = \phi$,

$$h(t) = \phi(0) + \int_{t_0}^t f(s, h_s) \, ds, \quad t \geq t_0. \quad (16)$$

We now provide existence and uniqueness result for the continuous-time τ -GRU model, assuming that the input x is continuous in t . Defining the state $h_t \in C$ as $h_t(\theta) := h(t + \theta)$ for $\theta \in [-\tau, 0]$ as before, the DDE describing the τ -GRU model can be formulated as the following IVP:

$$\dot{h} = -h(t) + u(t, h(t)) + a(t, h(t)) \odot z(t, h_t), \quad t \geq t_0, \quad (17)$$

and $h_{t_0} = \phi \in C$ for some initial time $t_0 \in \mathbb{R}$, with the dependence on $x(t)$ viewed as dependence on t . By applying Theorem 3.7 in [55], we can obtain the following result. See App. B for a proof of this theorem.

Theorem 1 (Existence and uniqueness of solution for continuous-time τ -GRU). *Let $t_0 \in \mathbb{R}$ and $\phi \in C$ be given. There exists a unique solution $h(t) = h(t, \phi)$ of Eq. (1), defined on $[t_0 - \tau, t_0 + A]$ for any $A > 0$. In particular, the solution exists for all $t \geq t_0$, and*

$$\|h_t(\phi) - h_t(\psi)\| \leq \|\phi - \psi\| e^{K(t-t_0)}, \quad (18)$$

for all $t \geq t_0$, where $K = 1 + \|W_1\| + \|W_2\| + \|W_4\|/4$.

Theorem 1 guarantees that the continuous-time τ -GRU model, as a functional differential equation, has a well-defined unique solution that does not blow up in finite time.

4.2 The Delay Mechanism in τ -GRUs Can Help Improve Long-Term Dependencies

RNNs suffer from the problem of vanishing and exploding gradients, leading to the problem of long-term dependencies. While the gating mechanisms could mitigate the problem to some extent, the delays introduced in τ -GRUs can further help reduce the sensitivity to long-term dependencies. To understand the reason for this, we consider how gradients are computed using the backpropagation through time (BPTT) algorithm [48]. BPTT involves the two stages of unfolding the network in time and backpropagating the training error through the unfolded network. When τ -GRUs are unfolded in time, the delays in the hidden state will appear as jump-ahead connections (buffers) in the unfolded network. These buffers provide a shorter path for propagating gradient information, and therefore reducing the sensitivity of the network to long-term dependencies. Such intuition is also used to explain the behavior of the NARX RNNs in [43].

We now make this intuition precise in the following simplified setting. See App. C for a proof of this proposition. We also provide analogous results (bounds for the gradient norm) and discussions for τ -GRU (in App. D, see Proposition 3).

Proposition 1. *Consider the linear time-delayed RNN whose hidden states are described by the update equation:*

$$h_{n+1} = Ah_n + Bh_{n-m} + Cu_n, \quad n = 0, 1, \dots, \quad (19)$$

and $h_n = 0$ for $n = -m, -m + 1, \dots, 0$ with $m > 0$. Then, assuming that A and B commute, we have:

$$\frac{\partial h_{n+1}}{\partial u_i} = A^{n-i} C, \quad (20)$$

for $n = 0, 1, \dots, m, i = 0, \dots, n$, and

$$\begin{aligned} \frac{\partial h_{m+1+j}}{\partial u_i} &= A^{m+j-i}C + \delta_{i,j-1}BC + 2\delta_{i,j-2}ABC \\ &\quad + 3\delta_{i,j-3}A^2BC + \dots + j\delta_{i,0}A^{j-1}BC, \end{aligned} \quad (21)$$

for $j = 1, 2, \dots, m + 1, i = 0, 1, \dots, m + j$, where $\delta_{i,j}$ denotes the Kronecker delta.

We remark that the commutativity assumption is not necessary. It is used here only to simplify the expression for the gradients. Analogous formula for the gradients can be derived without such assumption, at the cost of displaying more complicated formulae.

From Proposition 1, we see that the presence of the delay allows the model to place more emphasis on the gradients due to input information in the past (as can be seen in Eq. (38) in the proof of the proposition, where additional terms dependent on B appear in the coefficients in front of the past inputs). In particular, if $\|A\| < 1$ and $B = 0$, then the gradients decay exponentially as i becomes large. Introducing the delay term ($B \neq 0$) makes the rates at which this exponential decays lower by perturbing the gradients of hidden states (dependent on the delay parameter m) with respect to the past inputs with nonzero values.

Similar qualitative conclusion can also be drawn for our τ -GRU (see Proposition 3 and the discussions in App. D). Therefore, one expects that these networks would be able to more effectively deal with long-term dependencies than the counterpart models without delays.

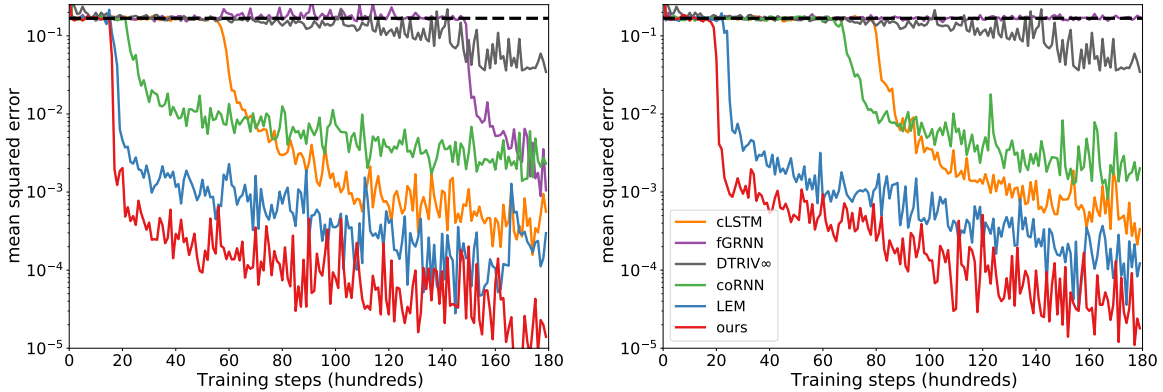
5 Experimental Results

In this section, we consider several benchmark datasets to demonstrate the performance of our proposed τ -GRU. We use standard protocols for training and initialization, and validation sets for parameter tuning (see App. F for details).

5.1 The Adding Task

The adding task is a classic problem for testing the ability of models to learn long-term dependencies, originally proposed by [24]. The inputs of this problem are composed of two stacked random vectors u and v of length N . The elements of u are drawn from the uniform distribution $\mathcal{U}(0, 1)$. The vector v has two non-zero elements (both set to 1), one placed in a random location i sampled from the index set $i \in \{1, \dots, \lfloor \frac{N}{2} \rfloor\}$, and the other element is placed at location j sampled from the index set $j \in \{\lceil \frac{N}{2} \rceil, \dots, N\}$. The target value for each sequence is constructed as the sum $\sum(u \odot v)$, i.e., the sum of the two elements in u that correspond to the non-negative entries v . Here, we follow the work by [53] and consider two challenging settings with very long input sequences $N = \{2000, 5000\}$.

Figure 2 shows results for our τ -GRU and several state-of-the-art RNN models which are designed to solve long-term dependencies tasks, such as LEM [53], coRNN [52], DTRIV $_{\infty}$ [38], fastGRNN [33], and LSTM with chrono



(a) Sequence length $N = 2000$.

(b) Sequence length $N = 5000$.

Figure 2: Results for the adding task on very long sequences.

initialization [57]. It can be seen that the DTRIV_∞ and fastGRNN are performing poorly in both cases. In contrast, our τ -GRU shows a favorable performance, i.e., τ -GRU is converging faster, and it achieves lower mean squared errors than other methods.

5.2 Sentiment Analysis: IMDB

Next, we consider the IMDB dataset [44] to study the expressiveness of our proposed model on a sentiment analysis task. The aim of this task is to predict whether a movie review is positive or negative. This dataset is composed of 50k movie reviews, with an average length of 240 words per review. Each review is annotated by a label that indicates a positive, or negative sentiment. The dataset is split evenly into a training and test set, so that both sets contain 25k reviews. We use 15% of the training data for validation. Further, we use standard preprocessing schemes, following [49], to restrict the dictionary to 25k words, and to embed the data with a pretrained GloVe model [49].

Table 1 shows that our τ -GRU achieves a substantially higher test accuracy than LSTM, and GRU models. Further, τ -GRU is also able to outperform the continuous-time coRNN [52] and the highly expressive LEM [53].

Table 1: Results for IMDB sentiment analysis task.

Model	Test Accuracy (%)	# units	# param
LSTM [10]	86.8	128	220k
Skip LSTM [10]	86.6	128	220k
GRU [10]	86.2	128	164k
Skip GRU [10]	86.6	128	164k
ReLU GRU [14]	84.8	128	99k
coRNN [52]	87.4	128	46k
LEM	88.1	128	220k
τ-GRU (ours)	88.6	128	220k

5.3 Human Activity Recognition: HAR-2

Here, we study the performance of our model for human activity recognition using the HAR dataset provided by [1]. This dataset consists of measurements by an accelerometer and gyroscope on a Samsung Galaxy S3 smartphone which are tracking six activities for 30 volunteers within an age bracket of 19-48 years. For learning, the sequences are divided into shorter sequences of length $N = 128$, and the raw measurements are summarized by 9 features per time step. Kusupati et al. [33] proposed the HAR-2 dataset which groups the activities into two categories {Sitting, Laying, Walking Upstairs} and {Standing, Walking, Walking Downstairs}. We use 7, 352 sequences for training, 900 for validation and 2, 947 for testing.

Table 2 shows that our τ -GRU is able to outperform traditional gated architectures on this task. The most competitive model is coRNN [52], which achieves a test accuracy of 97.2% with just 9k parameters. LEM [53] achieves 97.1% with the the same number of parameters as our τ -GRU.

Table 2: Results for HAR2 task.

Model	Test Accuracy (%)	# units	# param
GRU [33]	93.6	75	19k
LSTM [27]	93.7	64	19k
FastRNN [33]	94.5	80	7k
FastGRNN [33]	95.6	80	7k
AsymRNN [27]	93.2	120	8k
iRNN [27]	96.4	64	4k
DIRNN [65]	96.5	64	-
coRNN [52]	97.2	64	9k
LipschitzRNN	95.4	64	9k
LEM	97.1	64	19k
τ-GRU (ours)	97.4	64	19k

Table 3: Test accuracies on sMNIST, and psMNIST.

Model	sMNIST	psMNIST	# units	# parameters	sCIFAR	nCIFAR	# units	# parameters
LSTM [26]	97.8	92.6	128	68k	59.7	11.6	128	69k / 117k
r-LSTM [58]	98.4	95.2	-	100K	72.2	-	-	101k / -
chrono-LSTM [53]	98.9	94.6	128	68k	-	55.9	128	- / 116k
Antisymmetric RNN [11]	98.0	95.8	128	10k	62.2	54.7	256	37k / 37k
Lipschitz RNN [15]	99.4	96.3	128	34k	64.2	59.0	256	134k / 158k
exprNN [39]	98.4	96.2	360	68k	-	49.0	128	- / 47k
iRNN [27]	98.1	95.6	128	8k	-	54.5	128	- / 12k
TARNN [26]	98.9	97.1	128	68k	-	59.1	128	- / 100K
coRNN [52]	99.3	96.6	128	34k	-	59.0	128	- / 46k
LEM [53]	99.5	96.6	128	68k	-	60.5	128	- / 117k
Simple delay GRU (Eq. (12))	98.7	94.1	128	51k	57.2	59.8	128	52k / 75k
τ -GRU (ours)	99.4	97.3	128	68k	74.9	62.2	128	69k / 117k

5.4 Sequential Image Classification

Next, we consider four sequential variations of the MNIST [36] and CIFAR-10 [32] image classification datasets. These sequence classification tasks aim to evaluate the capability of RNNs to learn long-term dependencies.

The sequential MNIST (sMNIST) task, originally proposed by [35], is sequentially presenting the $N = 784$ pixels of each thumbnail to the recurrent unit. The final hidden state is used to predict the class membership probability of the flattened image. A variation of the sMNIST task is the permuted sMNIST task (psMNIST), which presents the model with a fixed random permutation of the pixel-by-pixel sequence. This task removes any natural patterns in the sequence and requires that models can learn long-term dependencies between pixels that are possibly far apart.

Since the standard sMNIST task has essentially been solved by state-of-the-art RNNs, [11] has proposed to consider the sequential CIFAR-10 (sCIFAR) task instead. This task is more challenging due to the increased sequence length, $N = 1024$, of the flattened input images. Each element of the sequence is a 3-dimensional vector that contains the pixels for each color channel. To solve this task, models require to have long-term memory and sufficient expressivity.

Furthermore, [11] has also proposed a noise-padded CIFAR-10 (nCIFAR) task, which requires that the RNN has the ability to memorize information from far in the past, and be able to suppress noisy segments that contain no relevant information. Specifically, we construct a sequence of length $N = 1000$ where each element is a 96-dimensional vector. The first 32 elements are the rows of an image, where the channels are stacked. The remaining 968 elements of the sequence are random vectors drawn from the standard normal distribution.

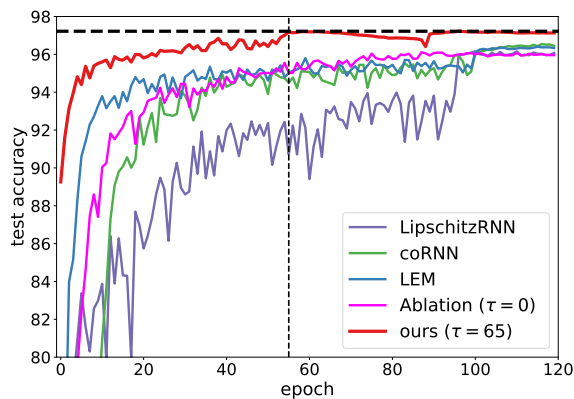


Figure 3: Test accuracy on permuted sequential MNIST as a function of the number of epochs. Our τ -GRU requires substantially fewer number of epochs to reach peak performance.

Table 3 shows results for the four described tasks. Our τ -GRU is competitive and able to outperform other models on the psMNIST, sCIFAR and nCIFAR task. The proposed weighted time-delay feedback mechanisms demonstrates a clear advantage in particular for the CIFAR tasks.

Figure 3 shows that our τ -GRU is converging faster than other recently introduced continuous-time models, such as LEM [53], coRNN [52], and LipschitzRNN [15]. This could help reduce training times when using these methods.

5.5 Ablation Study using psMNIST

We use the psMNIST task to perform an ablation study. To do so, we consider the following model

$$\mathbf{h}_{t+1} = (1 - \mathbf{g}_t) \odot \mathbf{h}_t + \mathbf{g}_t \odot (\beta \cdot \mathbf{u}_t + \alpha \cdot \mathbf{a}_t \odot \mathbf{z}_t)$$

where $\alpha \in [0, 1]$ and $\beta \in [0, 1]$ are constants that can be used to control the effect of different components. We are interested in the cases where α and β are either 0 or 1, i.e., a component is switched off or on.

Table 4 shows the results for different ablation configurations. By setting $\alpha = 0$ we yield a simple gated RNN. Second, for $\beta = 0$, we yield a τ -GRU without instantaneous dynamics. Third, we show how different values of τ affect the performance. Setting $\tau = 0$ leads to a τ -GRU without time-delay feedback. We also show that a model without the weighting function \mathbf{a}_t is not able to achieve peak performance.

Table 4: Ablation study.

Model	α	β	τ	\mathbf{a}_t	Test Accuracy (%)
ablation	0	1	-	yes	94.6
ablation	1	0	65	yes	94.9
ablation	1	1	0	yes	95.1
ablation	1	1	20	yes	96.4
ablation	1	1	65	no	96.8
τ-GRU (ours)	1	1	65	yes	97.3

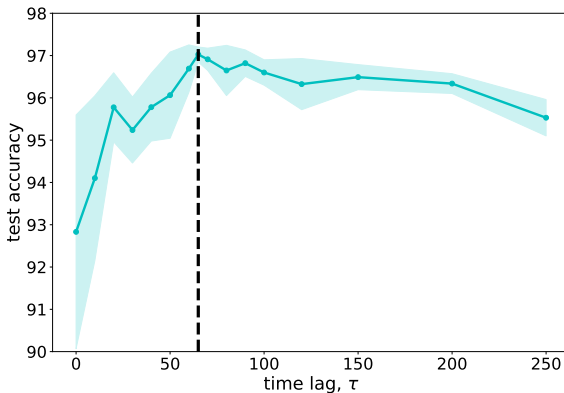


Figure 4: Sensitivity analysis of τ -GRU on psMNIST. The light green envelopes represent ± 1 standard deviation around the mean.

Figure 4 further investigates the effect of τ . The performance of τ -GRU is increasing as a function of τ and peaking around $\tau = 65$. It can be seen that the performance in the range $50 - 150$ is relatively constant for this task. Thus, the model is relatively insensitive as long as τ is sufficiently large, but not too large. The performance is starting to decrease for $\tau > 150$. Since τ takes discrete values, tuning is easier as compared to continuous tuning parameters, for instance, parameters used by LEM [53], coRNN [52], or LipschitzRNN [15].

5.6 Learning Climate Dynamics

We consider the task of learning the dynamics of the DDE model for El Niño Southern Oscillation (ENSO) of [19] (see Eq. (46) there). It models the sea surface temperature T in the eastern Pacific Ocean, and is described by:

$$\dot{T} = T - T^3 - cT(t - \delta)(1 - \gamma T^2(t - \delta)), \quad t > \delta, \quad (22)$$

where $\gamma < 1$, $c > 0$, with $T(t)$ satisfying $\dot{T} = T - T^3 - cT(0)(1 - \gamma T(0)^2)$ with $T(0) \sim \text{Unif}(0, 1)$ for $t \in [0, \delta]$. For data generation, we follow [19], and choose $c = 0.93$, $\gamma = 0.49$ and $\delta = 4.8$. We use the classical Runge-Kutta method (RK4) to numerically integrate the system from $t = 0$ to $t = 400$ using a step-size of 0.1. The training and testing samples are the time series (of length 2000) generated by the RK4 scheme on the interval [200, 400] for different realizations of $T(0)$.

Table 5 shows that our model (with $\alpha = \beta = 1$ and using $\tau = 20$) is more effective in learning the ENSO dynamics when compared to other RNN architectures. We also see that the predictive performance deteriorates without using appropriate combination of standard and delay recurrent units (setting either α or β to zero).

Table 5: Results for the ENSO model prediction.

Model	MSE ($\times 10^{-2}$)	# units	# parameters
Vanilla RNN	0.45	16	0.3k
LSTM	0.92	16	1.2k
GRU	0.53	16	0.9k
Lipschitz RNN	10.6	16	0.6k
coRNN	4.00	16	0.6k
LEM	0.31	16	1.2k
ablation ($\alpha = 0$)	0.31	16	0.6k
ablation ($\beta = 0$)	0.38	16	0.9k
τ-GRU (ours)	0.17	16	1.2k

6 Conclusion and Future Work

Starting from a continuous-time formulation, we derive a discrete-time gated recurrent unit with delay, τ -GRU. We also provide intuition and analysis to understand how the delay can act as a buffer to improve modeling of long-term dependencies. Importantly, we demonstrate the superior performance of τ -GRU in several challenging sequential learning tasks.

We now discuss some future directions. On the one hand, using multiple delays could lead to improved models, and therefore it is of interest to study the extension of τ -GRU to include suitable distributed delay mechanism. On the other hand, achieving model robustness with respect to adversarial perturbations and common corruptions is critical for sensitive applications, but it is largely unexplored in the sequential learning setting. It has been shown in [41, 42, 16] that noise injection can be effective in improving robustness. Therefore, it is also of interest to consider and study noise-injected versions of τ -GRU to improve the trade-offs between accuracy and robustness.

Acknowledgments

N. B. Erichson would like to acknowledge IARPA (contract W911NF20C0035). S. H. Lim would like to acknowledge the WINQ Fellowship, the Swedish Research Council (VR/2021-03648), and the computational resources provided by the Swedish National Infrastructure for Computing (SNIC) at Chalmers Centre for Computational Science and Engineering (C3SE) partially funded by the Swedish Research Council through grant agreement no. 2018-05973. M. W. Mahoney would also like to acknowledge NSF, and ONR for providing partial support of this work. Our conclusions do not necessarily reflect the position or the policy of our sponsors, and no official endorsement should be inferred.

References

- [1] Davide Anguita, Alessandro Ghio, Luca Oneto, Xavier Parra, and Jorge L Reyes-Ortiz. Human activity recognition on smartphones using a multiclass hardware-friendly support vector machine. In *International Workshop on Ambient Assisted Living*, pages 216–223. Springer, 2012. 8
- [2] Martin Arjovsky, Amar Shah, and Yoshua Bengio. Unitary evolution recurrent neural networks. In *International Conference on Machine Learning*, pages 1120–1128. PMLR, 2016. 3
- [3] Farshid Maghami Asl and A Galip Ulsoy. Analysis of a system of linear delay differential equations. *J. Dyn. Sys., Meas., Control*, 125(2):215–223, 2003. 4

- [4] Omri Azencot, N Benjamin Erichson, Mirela Ben-Chen, and Michael W Mahoney. A differential geometry perspective on orthogonal recurrent models. *arXiv preprint arXiv:2102.09589*, 2021. 3
- [5] Omri Azencot, N Benjamin Erichson, Vanessa Lin, and Michael Mahoney. Forecasting sequential data using consistent koopman autoencoders. In *International Conference on Machine Learning*, pages 475–485. PMLR, 2020. 3
- [6] Pierre Baldi and Amir F Atiya. How delays affect neural dynamics and learning. *IEEE Transactions on Neural Networks*, 5(4):612–621, 1994. 4
- [7] Andrew R Barron. Universal approximation bounds for superpositions of a sigmoidal function. *IEEE Transactions on Information theory*, 39(3):930–945, 1993. 22
- [8] Jacques Bélair. Stability in a model of a delayed neural network. *Journal of Dynamics and Differential Equations*, 5(4):607–623, 1993. 4
- [9] Sue Ann Campbell. Time delays in neural systems. In *Handbook of Brain Connectivity*, pages 65–90. Springer, 2007. 5
- [10] Víctor Campos, Brendan Jou, Xavier Giró-i Nieto, Jordi Torres, and Shih-Fu Chang. Skip RNN: Learning to skip state updates in recurrent neural networks. In *International Conference on Learning Representations*, 2018. 8
- [11] Bo Chang, Minmin Chen, Eldad Haber, and Ed H Chi. Antisymmetric RNN: A dynamical system view on recurrent neural networks. In *International Conference on Learning Representations*, 2018. 1, 3, 9, 23
- [12] Ricky TQ Chen, Yulia Rubanova, Jesse Bettencourt, and David K Duvenaud. Neural ordinary differential equations. *Advances in Neural Information Processing Systems*, 31, 2018. 3
- [13] Kyunghyun Cho, Bart Van Merriënboer, Dzmitry Bahdanau, and Yoshua Bengio. On the properties of neural machine translation: Encoder-decoder approaches. *arXiv preprint arXiv:1409.1259*, 2014. 2
- [14] Rahul Dey and Fathi M Salem. Gate-variants of gated recurrent unit (GRU) neural networks. In *2017 IEEE 60th International Midwest Symposium on Circuits and Systems (MWSCAS)*, pages 1597–1600. IEEE, 2017. 8
- [15] N Benjamin Erichson, Omri Azencot, Alejandro Queiruga, Liam Hodgkinson, and Michael W Mahoney. Lipschitz recurrent neural networks. In *International Conference on Learning Representations*, 2020. 1, 3, 9, 10, 23
- [16] N Benjamin Erichson, Soon Hoe Lim, Francisco Utrera, Winnie Xu, Ziang Cao, and Michael W Mahoney. NoisyMix: Boosting robustness by combining data augmentations, stability training, and noise injections. *arXiv preprint arXiv:2202.01263*, 2022. 11
- [17] N Benjamin Erichson, Michael Muehlebach, and Michael W Mahoney. Physics-informed autoencoders for lyapunov-stable fluid flow prediction. *arXiv preprint arXiv:1905.10866*, 2019. 3
- [18] Thomas Erneux. *Applied Delay Differential Equations*, volume 3. Springer, 2009. 4
- [19] Swinda KJ Falkena, Courtney Quinn, Jan Sieber, Jason Frank, and Henk A Dijkstra. Derivation of delay equation climate models using the Mori-Zwanzig formalism. *Proceedings of the Royal Society A*, 475(2227):20190075, 2019. 10, 11
- [20] Albert Gu, Isys Johnson, Karan Goel, Khaled Saab, Tri Dao, Atri Rudra, and Christopher Ré. Combining recurrent, convolutional, and continuous-time models with linear state space layers. *Advances in neural information processing systems*, 34:572–585, 2021. 3
- [21] Jack K Hale and Sjoerd M Verduyn Lunel. *Introduction to Functional Differential Equations*, volume 99. Springer Science & Business Media, 2013. 4, 6
- [22] Ramin Hasani, Mathias Lechner, Alexander Amini, Lucas Liebenwein, Aaron Ray, Max Tschaikowski, Gerald Teschl, and Daniela Rus. Closed-form continuous-time neural networks. *Nature Machine Intelligence*, pages 1–12, 2022. 3
- [23] Ramin Hasani, Mathias Lechner, Tsun-Hsuan Wang, Makram Chahine, Alexander Amini, and Daniela Rus. Liquid structural state-space models. *arXiv preprint arXiv:2209.12951*, 2022. 3
- [24] Sepp Hochreiter and Jürgen Schmidhuber. Long short-term memory. *Neural Computation*, 9(8):1735–1780, 1997. 2, 7
- [25] Herbert Jaeger, Mantas Lukoševičius, Dan Popovici, and Udo Siewert. Optimization and applications of echo state networks with leaky-integrator neurons. *Neural Networks*, 20(3):335–352, 2007. 5
- [26] Anil Kag and Venkatesh Saligrama. Time adaptive recurrent neural network. In *Proceedings of the IEEE/CVF Conference on Computer Vision and Pattern Recognition*, pages 15149–15158, 2021. 3, 9, 23
- [27] Anil Kag, Ziming Zhang, and Venkatesh Saligrama. RNNs incrementally evolving on an equilibrium manifold: A panacea for vanishing and exploding gradients? In *International Conference on Learning Representations*, 2020. 3, 8, 9, 23
- [28] Andrew Keane, Bernd Krauskopf, and Claire M Postlethwaite. Climate models with delay differential equations. *Chaos: An Interdisciplinary Journal of Nonlinear Science*, 27(11):114309, 2017. 4
- [29] Giancarlo Kerg, Kyle Goyette, Maximilian Puelma Touzel, Gauthier Gidel, Eugene Vorontsov, Yoshua Bengio, and Guillaume Lajoie. Non-normal recurrent neural network (nnRNN): Learning long time dependencies while improving expressivity with transient dynamics. In *Advances in Neural Information Processing Systems*,

- pages 13591–13601, 2019. [3](#)
- [30] Patrick Kidger, James Morrill, James Foster, and Terry Lyons. Neural controlled differential equations for irregular time series. *Advances in Neural Information Processing Systems*, 33:6696–6707, 2020. [3](#)
- [31] Sung-Suk Kim. Time-delay recurrent neural network for temporal correlations and prediction. *Neurocomputing*, 20(1-3):253–263, 1998. [3](#)
- [32] Alex Krizhevsky, Vinod Nair, and Geoffrey Hinton. CIFAR-10 (Canadian Institute for Advanced Research). [9](#)
- [33] Aditya Kusupati, Manish Singh, Kush Bhatia, Ashish Kumar, Prateek Jain, and Manik Varma. FastGRNN: A fast, accurate, stable and tiny kilobyte sized gated recurrent neural network. *Advances in Neural Information Processing Systems*, 31, 2018. [7](#), [8](#), [23](#)
- [34] Kevin J Lang, Alex H Waibel, and Geoffrey E Hinton. A time-delay neural network architecture for isolated word recognition. *Neural Networks*, 3(1):23–43, 1990. [3](#)
- [35] Quoc V. Le, Navdeep Jaitly, and Geoffrey E. Hinton. A simple way to initialize recurrent networks of rectified linear units. *arXiv preprint arXiv:1504.00941*, 2015. [9](#)
- [36] Yann LeCun, Léon Bottou, Yoshua Bengio, and Patrick Haffner. Gradient-based learning applied to document recognition. *Proceedings of the IEEE*, 86(11):2278–2324, 1998. [9](#)
- [37] S Lepri, G Giacomelli, A Politi, and FT Arcelli. High-dimensional chaos in delayed dynamical systems. *Physica D: Nonlinear Phenomena*, 70(3):235–249, 1994. [4](#)
- [38] Mario Lezcano Casado. Trivializations for gradient-based optimization on manifolds. *Advances in Neural Information Processing Systems*, 32, 2019. [3](#), [7](#)
- [39] Mario Lezcano-Casado and David Martinez-Rubio. Cheap orthogonal constraints in neural networks: A simple parametrization of the orthogonal and unitary group. *International Conference on Machine Learning*, pages 3794–3803, 2019. [3](#), [9](#), [23](#)
- [40] Xiaofeng Liao, Guanrong Chen, and Edgar N Sanchez. Delay-dependent exponential stability analysis of delayed neural networks: an LMI approach. *Neural Networks*, 15(7):855–866, 2002. [4](#)
- [41] Soon Hoe Lim, N Benjamin Erichson, Liam Hodgkinson, and Michael W Mahoney. Noisy recurrent neural networks. *Advances in Neural Information Processing Systems*, 34:5124–5137, 2021. [3](#), [11](#), [23](#)
- [42] Soon Hoe Lim, N Benjamin Erichson, Francisco Utrera, Winnie Xu, and Michael W Mahoney. Noisy feature mixup. *arXiv preprint arXiv:2110.02180*, 2021. [11](#)
- [43] Tsungnan Lin, Bill G Horne, Peter Tino, and C Lee Giles. Learning long-term dependencies in NARX recurrent neural networks. *IEEE Transactions on Neural Networks*, 7(6):1329–1338, 1996. [2](#), [3](#), [6](#)
- [44] Andrew Maas, Raymond E Daly, Peter T Pham, Dan Huang, Andrew Y Ng, and Christopher Potts. Learning word vectors for sentiment analysis. In *Proceedings of the 49th Annual Meeting of the Association for Computational Linguistics: Human Language Technologies*, pages 142–150, 2011. [8](#)
- [45] Michael C Mackey and Leon Glass. Oscillation and chaos in physiological control systems. *Science*, 197(4300):287–289, 1977. [24](#)
- [46] CM Marcus and RM Westervelt. Stability of analog neural networks with delay. *Physical Review A*, 39(1):347, 1989. [4](#)
- [47] Ju H Park, Tae H Lee, Yajuan Liu, and Jun Chen. *Dynamic Systems with Time Delays: Stability and Control*. Springer, 2019. [4](#)
- [48] Razvan Pascanu, Tomas Mikolov, and Yoshua Bengio. On the difficulty of training recurrent neural networks. In *International Conference on Machine Learning*, pages 1310–1318. PMLR, 2013. [2](#), [6](#), [18](#)
- [49] Jeffrey Pennington, Richard Socher, and Christopher D Manning. Glove: Global vectors for word representation. In *Proceedings of the 2014 conference on empirical methods in natural language processing (EMNLP)*, pages 1532–1543, 2014. [8](#)
- [50] Fernando J Pineda. Dynamics and architecture for neural computation. *Journal of Complexity*, 4(3):216–245, 1988. [1](#)
- [51] Alejandro Queiruga, N Benjamin Erichson, Liam Hodgkinson, and Michael W Mahoney. Stateful ode-nets using basis function expansions. *Advances in Neural Information Processing Systems*, 34:21770–21781, 2021. [3](#)
- [52] T. Konstantin Rusch and Siddhartha Mishra. Coupled oscillatory recurrent neural network (coRNN): An accurate and (gradient) stable architecture for learning long time dependencies. In *International Conference on Learning Representations*, 2021. [3](#), [7](#), [8](#), [9](#), [10](#), [23](#)
- [53] T. Konstantin Rusch, Siddhartha Mishra, N. Benjamin Erichson, and Michael W. Mahoney. Long expressive memory for sequence modeling. In *International Conference on Learning Representations*, 2022. [1](#), [3](#), [4](#), [7](#), [8](#), [9](#), [10](#), [22](#), [23](#)
- [54] Anton Maximilian Schäfer and Hans Georg Zimmermann. Recurrent neural networks are universal approximators. In *International Conference on Artificial Neural Networks*, pages 632–640, 2006. [21](#), [22](#)
- [55] Hal L Smith. *An Introduction to Delay Differential Equations with Applications to the Life Sciences*, volume 57. Springer New York, 2011. [4](#), [6](#), [16](#)

- [56] Jimmy TH Smith, Andrew Warrington, and Scott W Linderman. Simplified state space layers for sequence modeling. *arXiv preprint arXiv:2208.04933*, 2022. 3
- [57] Corentin Tallec and Yann Ollivier. Can recurrent neural networks warp time? In *International Conference on Learning Representations*, 2018. 4, 8
- [58] Trieu Trinh, Andrew Dai, Thang Luong, and Quoc Le. Learning longer-term dependencies in RNNs with auxiliary losses. In *International Conference on Machine Learning*, pages 4965–4974. PMLR, 2018. 9
- [59] Eugene Vorontsov, Chiheb Trabelsi, Samuel Kadoury, and Chris Pal. On orthogonality and learning recurrent networks with long term dependencies. In *International Conference on Machine Learning*, pages 3570–3578. PMLR, 2017. 3
- [60] Alexander Waibel, Toshiyuki Hanazawa, Geoffrey Hinton, Kiyohiro Shikano, and Kevin J Lang. Phoneme recognition using time-delay neural networks. *IEEE Transactions on Acoustics, Speech, and Signal Processing*, 37(3):328–339, 1989. 3
- [61] Pete Warden. Speech commands: A dataset for limited-vocabulary speech recognition. *arXiv preprint arXiv:1804.03209*, 2018. 3, 23
- [62] Scott Wisdom, Thomas Powers, John Hershey, Jonathan Le Roux, and Les Atlas. Full-capacity unitary recurrent neural networks. *Advances in Neural Information Processing Systems*, 29, 2016. 3
- [63] Hedi Xia, Vai Suliafu, Hangjie Ji, Tan Nguyen, Andrea Bertozzi, Stanley Osher, and Bao Wang. Heavy ball neural ordinary differential equations. *Advances in Neural Information Processing Systems*, 34:18646–18659, 2021. 3
- [64] Zhichun Yang, Weisong Zhou, and Tingwen Huang. Exponential input-to-state stability of recurrent neural networks with multiple time-varying delays. *Cognitive Neurodynamics*, 8(1):47–54, 2014. 4
- [65] Ziming Zhang, Guojun Wu, Yanhua Li, Yun Yue, and Xun Zhou. Deep incremental RNN for learning sequential data: A Lyapunov stable dynamical system. In *2021 IEEE International Conference on Data Mining (ICDM)*, pages 966–975. IEEE, 2021. 8
- [66] Qunxi Zhu, Yao Guo, and Wei Lin. Neural delay differential equations. *arXiv preprint arXiv:2102.10801*, 2021. 3

Appendix

This Appendix is organized as follows. In Section A, we provide illustrations to demonstrate the differences between input-driven ODE and DDE dynamics in the scalar setting. In Section B, we provide the proof of Theorem 1. In Section C, we provide proof of Proposition 1. In Section D, we provide gradient bounds for τ -GRU. In Section E, we provide a universal approximation result for a general class of time-delayed RNNs. In Section F, we provide additional experimental results and details.

We are using the following notation throughout this appendix: \odot denotes Hadamard product, $|v|$ (or $\|v\|$) denotes vector norm for the vector v , $\|A\|$ denotes operator norm for the matrix A , $\|A\|_\infty$ denotes the matrix norm induced by ∞ -norm (i.e., maximum absolute row sum of the matrix A), σ and $\hat{\sigma}$ (or sigmoid) denote the tanh and sigmoid function, respectively, and $\lceil x \rceil$ and $\lfloor x \rfloor$ denote the ceiling function and floor function in x , respectively. In addition, $\delta_{i,j}$ denotes the Kronecker delta, i.e., $\delta_{i,j} = 1$ if $i = j$ and $\delta_{i,j} = 0$ if $i \neq j$.

A Illustrations of Differences Between ODE and DDE Dynamics

Of particular interest to us are the differences between ODEs and DDEs that are driven by an input. To illustrate the differences in the context of RNNs in terms of how they map the input signal into an output signal, we consider the simple examples:

- (a) DDE based RNNs with the hidden states $h \in \mathbb{R}$ satisfying $\dot{h} = -h(t - \tau) + u(t)$, with $\tau = 0.5$ and $\tau = 1$, and $h(t) = 0$ for $t \in [-\tau, 0]$, and
- (b) an ODE based RNN with the hidden states $h \in \mathbb{R}$ satisfying $\dot{h} = -h(t) + u(t)$,

where $u(t) = \cos(t)$ is the driving input signal.

Figure 5 shows the difference between the dynamics of the hidden state driven by the input signal for (a) and (b). We see that, when compared to the ODE based RNN, the introduced delay causes time lagging in the response of the RNNs to the input signal. The responses are also amplified. In particular, using $\tau = 0.5$ makes the response of the RNN closely matches the input signal. In other words, simply fine tuning the delay parameter τ in the scalar RNN model is sufficient to replicate the dynamics of the input signal.

To further illustrate the differences, we consider the following examples of RNN with a nonlinear activation:

- (c) DDE based RNNs with the hidden states $h \in \mathbb{R}$ satisfying $\dot{h} = -h + \tanh(-h(t - \tau) + s(t))$, with $\tau > 0$, and $h(t) = 0$ for $t \in [-\tau, 0]$, and
- (d) an ODE based RNN with the hidden states $h \in \mathbb{R}$ satisfying $\dot{h} = -h + \tanh(-h(t) + s(t))$,

where the driving input signal s is taken to be the truncated Weierstrass function:

$$s(t) = \sum_{n=0}^3 a^{-n} \cos(b^n \cdot \omega t), \quad (23)$$

where $a = 3$, $b = 4$ and $\omega = 2$.

Figure 6 shows the difference between the input-driven dynamics of the hidden states for (c) and (d). We see that, when compared to the ODE based RNN, the introduced delay causes time lagging in the response of the RNNs to the input signal. Even though the response of both RNNs does not match the input signal precisely (since we consider RNNs with one-dimensional hidden states here and therefore their expressivity is limited), we see that using $\tau = 0.5$ produces a response that tracks the seasonality of the input signal better than the ODE based RNN.

B Proof of Theorem 1

In this section, we provide a proof of Theorem 1. To start, note that one can view the solution of the DDE as a mapping of functions on the interval $[t - \tau, t]$ into functions on the interval $[t, t + \tau]$, i.e., as a sequence of functions defined over a set of contiguous time intervals of length τ . This perspective makes it more straightforward to prove existence and uniqueness theorems analogous to those for ODEs than by directly viewing DDEs as an evolution over the state space \mathbb{R}^d .

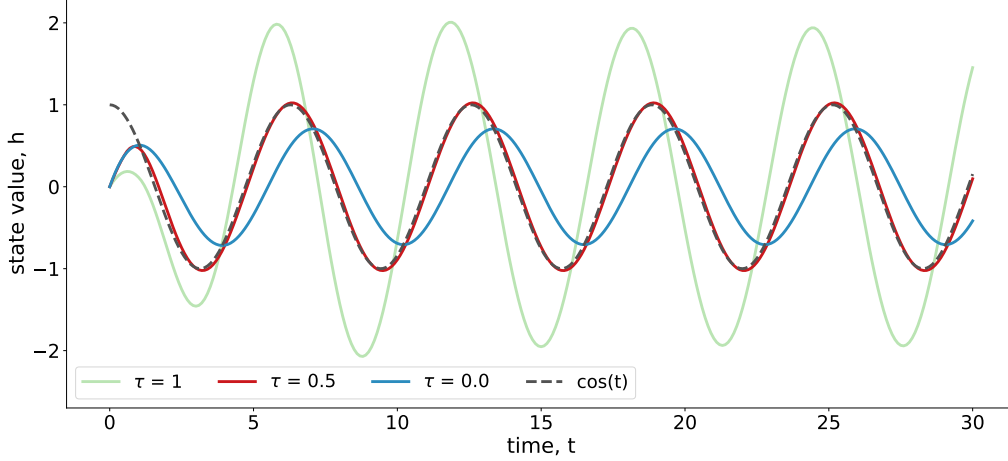


Figure 5: Hidden state dynamics of the DDE based RNNs with $\tau = 0.5$ and $\tau = 1$, and the ODE based RNN ($\tau = 0$). All RNNs are driven by the same cosine input signal.

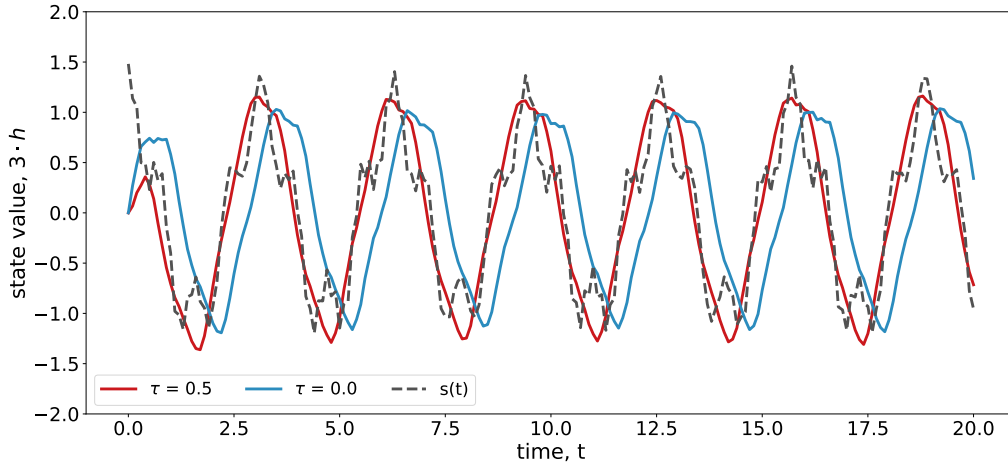


Figure 6: Hidden state dynamics of the DDE based RNN with $\tau = 0.5$ and the ODE based RNN ($\tau = 0$). All RNNs are driven by the same input signal $s(t)$.

The following theorem, adapted from Theorem 3.7 in [55], provides sufficient conditions for existence and uniqueness of solution through a point $(t_0, \phi) \in \mathbb{R} \times C$ for the IVP (15). Recall that $C := C([-\tau, 0], \mathbb{R}^d)$, the Banach space of continuous functions from $[-\tau, 0]$ into \mathbb{R}^d with the topology of uniform convergence. It is equipped with the norm $\|\phi\| := \sup\{|\phi(\theta)| : \theta \in [-\tau, 0]\}$.

Theorem 2 (Adapted from Theorem 3.7 in [55]). *Let $t_0 \in \mathbb{R}$ and $\phi \in C$ be given. Assume that f is continuous and satisfies the Lipschitz condition on each bounded subset of $\mathbb{R} \times C$, i.e., for all $a, b \in \mathbb{R}$, there exists a constant $K > 0$ such that*

$$|f(t, \phi) - f(t, \psi)| \leq K\|\phi - \psi\|, \quad t \in [a, b], \quad \|\phi\|, \|\psi\| \leq M, \quad (24)$$

with K possibly dependent on a, b, M .

There exists $A > 0$, depending only on M such that if $\phi \in C$ satisfies $\|\phi\| \leq M$, then there exists a unique solution $h(t) = h(t, \phi)$ of Eq. (15), defined on $[t_0 - \tau, t_0 + A]$. Moreover, if K is the Lipschitz constant for f corresponding to $[t_0, t_0 + A]$ and M , then

$$\max_{\eta \in [t_0 - \tau, t_0 + A]} |h(\eta, \phi) - h(\eta, \psi)| \leq \|\phi - \psi\| e^{KA}, \quad \|\phi\|, \|\psi\| \leq M. \quad (25)$$

We now provide existence and uniqueness result for the continuous-time τ -GRU model, assuming that the input x is continuous in t . As before, we define the state $h_t \in C$ as:

$$h_t(\theta) := h(t + \theta), \quad -\tau \leq \theta \leq 0. \quad (26)$$

Then the DDE defining the model can be formulated as the following IVP for the nonautonomous system:

$$\dot{h}(t) = -h(t) + u(t, h(t)) + a(t, h(t)) \odot z(t, h_t), \quad t \geq t_0, \quad (27)$$

and $h_{t_0} = \phi \in C$ for some initial time $t_0 \in \mathbb{R}$, with the dependence on $x(t)$ casted as dependence on t for notational convenience.

Now we restate Theorem 1 from the main text and provide the proof.

Theorem 3 (Existence and uniqueness of solution for continuous-time τ -GRU). *Let $t_0 \in \mathbb{R}$ and $\phi \in C$ be given. There exists a unique solution $h(t) = h(t, \phi)$ of Eq. (27), defined on $[t_0 - \tau, t_0 + A]$ for any $A > 0$. In particular, the solution exists for all $t \geq t_0$, and*

$$\|h_t(\phi) - h_t(\psi)\| \leq \|\phi - \psi\| e^{K(t-t_0)}, \quad (28)$$

for all $t \geq t_0$, where $K = 1 + \|W_1\| + \|W_2\| + \|W_4\|/4$.

Proof. We shall apply Theorem 2. To verify the Lipschitz condition: for any $\phi, \psi \in C$,

$$\begin{aligned} & |(u(t, \phi) + a(t, \phi) \odot z(t, \phi) - \phi) - (u(t, \psi) + a(t, \psi) \odot z(t, \psi) - \psi)| \\ & \leq |u(t, \phi) - u(t, \psi)| + |\phi - \psi| + |(a(t, \phi) - a(t, \psi)) \odot z(t, \phi)| + |a(t, \psi) \odot (z(t, \phi) - z(t, \psi))| \end{aligned} \quad (29)$$

$$\leq \|W_1\| \cdot |\phi - \psi| + |\phi - \psi| + \frac{1}{4} \|W_4\| \cdot |\phi - \psi| + \|W_2\| \cdot |\phi - \psi| \quad (30)$$

$$=: K|\phi - \psi|, \quad (31)$$

where we have used the fact that the tanh and sigmoid are Lipschitz continuous, both bounded by one in absolute value, and they have positive derivatives of magnitude no larger than one and 1/4 respectively in the last inequality above.

Therefore, we see that the right hand side function satisfies a global Lipschitz condition and so the result follows from Theorem 2. \square

C Proof of Proposition 1

In this section, we restate Proposition 1, and provide its proof and some remarks.

Proposition 2. *Consider the linear time-delayed RNN whose hidden states are described by the update equation:*

$$h_{n+1} = Ah_n + Bh_{n-m} + Cu_n, \quad n = 0, 1, \dots, \quad (32)$$

and $h_n = 0$ for $n = -m, -m + 1, \dots, 0$ with $m > 0$. Then, assuming that A and B commute, we have:

$$\frac{\partial h_{n+1}}{\partial u_i} = A^{n-i}C, \quad (33)$$

for $n = 0, 1, \dots, m$, $i = 0, \dots, n$, and

$$\begin{aligned} \frac{\partial h_{m+1+j}}{\partial u_i} &= A^{m+j-i}C + \delta_{i,j-1}BC + 2\delta_{i,j-2}ABC \\ &\quad + 3\delta_{i,j-3}A^2BC + \dots + j\delta_{i,0}A^{j-1}BC, \end{aligned} \quad (34)$$

for $j = 1, 2, \dots, m + 1$, $i = 0, 1, \dots, m + j$, where $\delta_{i,j}$ denotes the Kronecker delta.

Proof. Note that by definition $h_i = 0$ for $i = -m, -m + 1, \dots, 0$, and, upon iterating the recursion (32), one obtains:

$$h_{n+1} = A^nCu_0 + A^{n-1}Cu_1 + \dots + ACu_{n-1} + Cu_n, \quad (35)$$

for $n = 0, 1, \dots, m$.

Now, applying the above formula for h_1 , we obtain

$$\begin{aligned} h_{m+2} &= Ah_{m+1} + Bh_1 + Cu_{m+1} \\ &= (B + A^{m+1})Cu_0 + A^mCu_1 + \cdots + A^2Cu_{m-1} + ACu_m + Cu_{m+1}. \end{aligned} \quad (36)$$

Likewise, we obtain:

$$\begin{aligned} h_{m+3} &= Ah_{m+2} + Bh_2 + Cu_{m+2} \\ &= (BA + A^{m+2} + AB)Cu_0 + (B + A^{m+1})Cu_1 + A^mCu_2 + \cdots + ACu_{m+1} + Cu_{m+2} \\ &= (2AB + A^{m+2})Cu_0 + (B + A^{m+1})Cu_1 + A^mCu_2 + \cdots + ACu_{m+1} + Cu_{m+2}, \end{aligned} \quad (37)$$

where we have used commutativity of A and B in the last line above.

Applying the above procedure repeatedly and using commutativity of A and B give:

$$h_{m+1+j} = (A^{m+j} + jA^{j-1}B)Cu_0 + (A^{m+j-1} + (j-1)A^{j-2}B)Cu_1 + \cdots + ACu_{m+j-1} + Cu_{m+j}, \quad (38)$$

for $j = 1, 2, \dots, m+1$.

The formula in the proposition then follows upon taking the derivative with respect to the u_i in the above formula for the hidden states h_k . \square

We remark that one could also derive formula for the gradients $\frac{\partial h_{n+1+j}}{\partial u_i}$ for $n \geq 2m+1$ as well as those for our τ -GRU architecture analogously, albeit the resulting expression is quite complicated. In particular, the dependence on higher powers of B for the coefficients in front of the Kronecker deltas would appear in the formula for the former case (with much more complicated expressions without assuming commutativity of the matrices). However, we emphasize that the qualitative conclusion derived from the analysis remains the same: that introduction of delays places more emphasis on gradient information due to input elements in the past, so they act as buffers to propagate the gradient information more effectively than the counterpart models without delays.

D Gradient Bounds for τ -GRU

On the exploding and vanishing gradient problem. For simplicity of our discussion here, we consider the loss function:

$$\mathcal{E}_n = \frac{1}{2} \|y_n - \bar{y}_n\|^2, \quad (39)$$

where $n = 1, \dots, N$ and \bar{y}_n denotes the underlying growth truth. The training of τ -GRU involves computing gradients of this loss function with respect to its underlying parameters $\theta \in \Theta = [W_{1,2,3,4}, U_{1,2,3,4}, V]$ at each iteration of the gradient descent algorithm. Using chain rule, we obtain [48]:

$$\frac{\partial \mathcal{E}_n}{\partial \theta} = \sum_{k=1}^n \frac{\partial \mathcal{E}_n^{(k)}}{\partial \theta}, \quad (40)$$

where

$$\frac{\partial \mathcal{E}_n^{(k)}}{\partial \theta} = \frac{\partial \mathcal{E}_n}{\partial h_n} \frac{\partial h_n}{\partial h_k} \frac{\partial^+ h_k}{\partial \theta}, \quad (41)$$

with $\frac{\partial^+ h_k}{\partial \theta}$ denoting the ‘‘immediate’’ partial derivative of the state h_k with respect to θ , i.e., where h_{k-1} is taken as a constant with respect to θ [48].

The partial gradient $\frac{\partial \mathcal{E}_n^{(k)}}{\partial \theta}$ measures the contribution to the hidden state gradient at step n due to the information at step k . It can be shown that this gradient behaves as

$$\frac{\partial \mathcal{E}_n^{(k)}}{\partial \theta} \sim \gamma^{n-k}, \quad (42)$$

for some $\gamma > 0$ [48]. If $\gamma > 1$, then the gradient grows exponentially in sequence length, for long-term dependencies where $k \ll n$, causing the exploding gradient problem. On the other hand, if $\gamma < 1$, then the gradient decays exponentially for $k \ll n$, causing the vanishing gradient problem. Therefore, we can investigate how τ -GRU deals

with these problems by deriving bounds on the gradients. In particular, we are interested in the behavior of the gradients for long-term dependencies, i.e., $k \ll n$, and shall show that the delay mechanism in τ -GRU slows down the exponential decay rate, thereby reducing the sensitivity to the vanishing gradient problem.

Recall that the update equations defining τ -GRU are given by $h_n = 0$ for $n = -m, -m + 1, \dots, 0$,

$$h_n = (1 - g(A_{n-1})) \odot h_{n-1} + g(A_{n-1}) \odot [u(B_{n-1}) + a(C_{n-1}) \odot z(D_{n-m-1})], \quad (43)$$

for $n = 1, 2, \dots, N$, where $m := \lfloor \tau / \Delta t \rfloor \in \{1, 2, \dots, N - 1\}$, $A_{n-1} = W_3 h_{n-1} + U_3 x_{n-1}$, $B_{n-1} = W_1 h_{n-1} + U_1 x_{n-1}$, $C_{n-1} = W_4 h_{n-1} + U_4 x_{n-1}$, and $D_{n-m-1} = W_2 h_{n-m-1} + U_2 x_{n-1}$.

In the sequel, we shall denote the i th component of a vector v as v^i and the (i, j) entry of a matrix A as A^{ij} .

We start with the following lemma.

Lemma 1. *For every i , we have $h_n^i = 0$, for $n = -m, -m + 1, \dots, 0$, and $|h_n^i| \leq 2$, for $n = 1, 2, \dots, N$.*

Proof. The i th component of the hidden states of τ -GRU are given by: $h_n^i = 0$ for $n = -m, -m + 1, \dots, 0$, and

$$h_n^i = (1 - g(A_{n-1}^i)) h_{n-1}^i + g(A_{n-1}^i) [u(B_{n-1}^i) + a(C_{n-1}^i) z(D_{n-m-1}^i)], \quad (44)$$

for $n = 1, 2, \dots, N$.

Using the fact that $g(x), a(x) \in (0, 1)$ and $u(x), z(x) \in (-1, 1)$ for all x , we can bound the h_n^i as:

$$\begin{aligned} h_n^i &\leq (1 - g(A_{n-1}^i)) \max(h_{n-1}^i, 2) + g(A_{n-1}^i) \max(h_{n-1}^i, 2) \\ &\leq \max(h_{n-1}^i, 2), \end{aligned} \quad (45)$$

for all i and $n = 1, 2, \dots, N$.

Similarly, we have:

$$\begin{aligned} h_n^i &\geq (1 - g(A_{n-1}^i)) \min(-2, h_{n-1}^i) + g(A_{n-1}^i) \min(-2, h_{n-1}^i) \\ &\geq \min(-2, h_{n-1}^i), \end{aligned} \quad (46)$$

for all i and $n = 1, 2, \dots, N$.

Thus,

$$\min(-2, h_{n-1}^i) \leq h_n^i \leq \max(h_{n-1}^i, 2), \quad (47)$$

for all i and $n = 1, 2, \dots, N$.

Now, iterating over n and using $h_0^i = 0$ for all i , we obtain $-2 \leq h_n^i \leq 2$ for all i and $n = 1, 2, \dots, N$. \square

We now provide the gradients bound for τ -GRU in the following proposition and proof.

Proposition 3. *Assume that there exists an $\epsilon > 0$ such that $\max_n g(A_{n-1}^i) \geq \epsilon$ and $\max_n a(C_{n-1}^i) \geq \epsilon$ for all i . Then*

$$\left\| \frac{\partial h_n}{\partial h_k} \right\|_{\infty} \leq (1 + C - \epsilon)^{n-k} + \|W_2\|_{\infty} \cdot ((1 + C - \epsilon)^{n-k-2} \delta_{m,1} + \dots + (1 + C - \epsilon) \delta_{m,n-k-2} + \delta_{m,n-k-1}), \quad (48)$$

for $n = 1, \dots, N$ and $k < n$, where $C = \|W_1\|_{\infty} + \|W_3\|_{\infty} + \frac{1}{4} \|W_4\|_{\infty}$.

Proof. Recall $h_n = 0$ for $n = -m, -m + 1, \dots, 0$, and

$$h_n = (1 - g(A_{n-1})) \odot h_{n-1} + g(A_{n-1}) \odot [u(B_{n-1}) + a(C_{n-1}) \odot z(D_{n-m-1})] =: F(h_{n-1}, h_{n-m-1}), \quad (49)$$

for $n = 1, 2, \dots, N$.

Denote $q_{n,l} := \frac{\partial F}{\partial h_{n-l}}$, where $F := F(h_{n-1}, h_{n-1})$ for $l > 1$. The gradients $\frac{\partial h_n}{\partial h_k}$ can be computed recursively as follows.

$$p_n^{(1)} := \frac{\partial h_n}{\partial h_{n-1}}, \quad (50)$$

$$p_n^{(2)} := \frac{\partial h_n}{\partial h_{n-2}} = p_n^{(1)} p_{n-1}^{(1)} + q_{n,2} \delta_{m,1}, \quad (51)$$

$$p_n^{(3)} := \frac{\partial h_n}{\partial h_{n-3}} = p_n^{(1)} p_{n-1}^{(2)} + q_{n,3} \delta_{m,2}, \quad (52)$$

$$\vdots \quad (53)$$

$$p_n^{(n-k)} := \frac{\partial h_n}{\partial h_k} = p_n^{(1)} p_{n-1}^{(n-k-1)} + q_{n,n-k} \delta_{m,n-k-1}. \quad (54)$$

As $\|p_n^{(n-k)}\| \leq \|p_n^{(1)}\| \cdot \|p_{n-1}^{(n-k-1)}\| + \|q_{n,n-k}\| \delta_{m,n-k-1}$, it remains to upper bound the $p_n^{(1)}$ and $q_{n,n-k}$.

The i th component of the hidden states can be written as:

$$h_n^i = (1 - g(A_{n-1}^i)) h_{n-1}^i + g(A_{n-1}^i) [u(B_{n-1}^i) + a(C_{n-1}^i) z(D_{n-m-1}^i)], \quad (55)$$

where $A_{n-1}^i = W_3^{iq} h_{n-1}^q + U_3^{ir} x_{n-1}^r$, $B_{n-1}^i = W_1^{iq} h_{n-1}^q + U_1^{ir} x_{n-1}^r$, $C_{n-1}^i = W_4^{iq} h_{n-1}^q + U_4^{ir} x_{n-1}^r$, and $D_{n-m-1}^i = W_2^{iq} h_{n-m-1}^q + U_2^{ir} x_{n-1}^r$, using Einstein's summation notation for repeated indices.

Therefore, applying chain rule and using Einstein's summation for repeated indices in the following, we obtain:

$$\begin{aligned} \frac{\partial h_n^i}{\partial h_{n-1}^j} &= (1 - g(A_{n-1}^i)) \frac{\partial h_{n-1}^i}{\partial h_{n-1}^j} - \frac{\partial g(A_{n-1}^i)}{\partial A_{n-1}^l} \frac{\partial A_{n-1}^l}{\partial h_{n-1}^j} h_{n-1}^i + g(A_{n-1}^i) \frac{\partial u(B_{n-1}^i)}{\partial B_{n-1}^l} \frac{\partial B_{n-1}^l}{\partial h_{n-1}^j} \\ &\quad + \frac{\partial g(A_{n-1}^i)}{\partial A_{n-1}^l} \frac{\partial A_{n-1}^l}{\partial h_{n-1}^j} u(B_{n-1}^i) + g(A_{n-1}^i) \frac{\partial a(C_{n-1}^i)}{\partial C_{n-1}^l} \frac{\partial C_{n-1}^l}{\partial h_{n-1}^j} z(D_{n-m-1}^i) \\ &\quad + \frac{\partial g(A_{n-1}^i)}{\partial A_{n-1}^l} \frac{\partial A_{n-1}^l}{\partial h_{n-1}^j} a(C_{n-1}^i) z(D_{n-m-1}^i). \end{aligned} \quad (56)$$

Noting that $\frac{\partial g(A_{n-1}^i)}{\partial A_{n-1}^l} = 0$, $\frac{\partial u(B_{n-1}^i)}{\partial B_{n-1}^l} = 0$ and $\frac{\partial a(C_{n-1}^i)}{\partial C_{n-1}^l} = 0$ for $i \neq l$, we have:

$$\begin{aligned} \frac{\partial h_n^i}{\partial h_{n-1}^j} &= (1 - g(A_{n-1}^i)) \frac{\partial h_{n-1}^i}{\partial h_{n-1}^j} - \frac{\partial g(A_{n-1}^i)}{\partial A_{n-1}^i} \frac{\partial A_{n-1}^i}{\partial h_{n-1}^j} h_{n-1}^i + g(A_{n-1}^i) \frac{\partial u(B_{n-1}^i)}{\partial B_{n-1}^i} \frac{\partial B_{n-1}^i}{\partial h_{n-1}^j} \\ &\quad + \frac{\partial g(A_{n-1}^i)}{\partial A_{n-1}^i} \frac{\partial A_{n-1}^i}{\partial h_{n-1}^j} u(B_{n-1}^i) + g(A_{n-1}^i) \frac{\partial a(C_{n-1}^i)}{\partial C_{n-1}^i} \frac{\partial C_{n-1}^i}{\partial h_{n-1}^j} z(D_{n-m-1}^i) \\ &\quad + \frac{\partial g(A_{n-1}^i)}{\partial A_{n-1}^i} \frac{\partial A_{n-1}^i}{\partial h_{n-1}^j} a(C_{n-1}^i) z(D_{n-m-1}^i) \end{aligned} \quad (57)$$

$$\begin{aligned} &= (1 - g(A_{n-1}^i)) \delta_{i,j} - \frac{\partial g(A_{n-1}^i)}{\partial A_{n-1}^i} W_3^{ij} h_{n-1}^i + g(A_{n-1}^i) \frac{\partial u(B_{n-1}^i)}{\partial B_{n-1}^i} W_1^{ij} \\ &\quad + \frac{\partial g(A_{n-1}^i)}{\partial A_{n-1}^i} W_3^{ij} u(B_{n-1}^i) + g(A_{n-1}^i) \frac{\partial a(C_{n-1}^i)}{\partial C_{n-1}^i} W_4^{ij} z(D_{n-m-1}^i) \\ &\quad + \frac{\partial g(A_{n-1}^i)}{\partial A_{n-1}^i} W_3^{ij} a(C_{n-1}^i) z(D_{n-m-1}^i). \end{aligned} \quad (58)$$

Using the assumption that $\max_n g(A_{n-1}^i), \max_n a(C_{n-1}^i) \geq \epsilon$ for all i , the fact that $|z(x)|, |u(x)| \leq 1$, $g(x), a(x) \in (0, 1)$, $g'(x), a'(x) \leq 1/4$, $u'(x) \leq 1$ for all $x \in \mathbb{R}$, and Lemma 1, we obtain:

$$\left| \frac{\partial h_n^i}{\partial h_{n-1}^j} \right| \leq (1 - \epsilon) \delta_{i,j} + \frac{1}{4} |W_3^{ij}| \cdot |h_{n-1}^i| + |W_1^{ij}| + \frac{1}{4} |W_3^{ij}| + \frac{1}{4} |W_4^{ij}| + \frac{1}{4} |W_3^{ij}| \quad (59)$$

$$\leq (1 - \epsilon) \delta_{i,j} + |W_1^{ij}| + |W_3^{ij}| + \frac{1}{4} |W_4^{ij}|. \quad (60)$$

Therefore,

$$\left\| \frac{\partial h_n}{\partial h_{n-1}} \right\|_\infty := \max_{i=1, \dots, d} \sum_{j=1}^d \left| \frac{\partial h_n^i}{\partial h_{n-1}^j} \right| \leq (1 - \epsilon) + \|W_1\|_\infty + \|W_3\|_\infty + \frac{1}{4} \|W_4\|_\infty =: 1 - \epsilon + C. \quad (61)$$

Likewise, we obtain, for $l > 1$:

$$\frac{\partial F^i}{\partial h_{n-l}^j} = g(A_{n-1}^i) a(C_{n-1}^i) \frac{\partial z(D_{n-l}^i)}{\partial D_{n-l}^i} \frac{\partial D_{n-l}^i}{\partial h_{n-l}^j} \quad (62)$$

$$= g(A_{n-1}^i) a(C_{n-1}^i) \frac{\partial z(D_{n-l}^i)}{\partial D_{n-l}^i} W_2^{ij}. \quad (63)$$

Using the fact that $|g(x)|, |a(x)| \leq 1$ and $|z'(x)| \leq 1$ for all $x \in \mathbb{R}$, we obtain:

$$\left| \frac{\partial F^i}{\partial h_{n-l}^j} \right| \leq |W_2^{ij}|, \quad (64)$$

for $l > 1$, and thus $\|q_{n,n-k}\|_\infty = \left\| \frac{\partial F}{\partial h_k} \right\|_\infty \leq \|W_2\|_\infty$ for $k > 1$.

The upper bound in the proposition follows by using the above bounds for $\|p_n^{(1)}\|_\infty$ and $\|q_{n,n-k}\|_\infty$, and iterating the recursion $\|p_n^{(n-k)}\| \leq \|p_n^{(1)}\| \cdot \|p_{n-1}^{(n-k-1)}\| + \|q_{n,n-k}\| \delta_{m,n-k-1}$ over k . \square

From Proposition 3, we see that if $\epsilon > C$, then the gradient norm decays exponentially as k becomes large. However, the delay in τ -GRU introduces jump-ahead connections (buffers) to slow down the exponential decay. For instance, choosing $m = 1$ for the delay, we have $\left\| \frac{\partial h_n}{\partial h_k} \right\| \sim (1 + C - \epsilon)^{n-k-2}$ as $k \rightarrow \infty$ (instead of $\left\| \frac{\partial h_n}{\partial h_k} \right\| \sim (1 + C - \epsilon)^{n-k-1}$ as $k \rightarrow \infty$ in the case when no delay is introduced into the model). The larger the m is, the more effective the delay is able to slow down the exponential decay of the gradient norm. These qualitative conclusions can already be derived by studying the linear time-delayed RNN, which we consider in the main text for simplicity.

E Approximation Capability of Time-Delayed RNNs

RNNs (without delay) have been shown to be universal approximators of a large class of open dynamical systems [54]. Analogously, RNNs with delay can be shown to be universal approximators of open dynamical systems with delay.

Let $m > 0$ (time lag) and consider the state space models (which, in this section, we shall simply refer to as delayed RNNs) of the form:

$$\begin{aligned} s_{n+1} &= f(As_n + Bs_{n-m} + Cu_n + b), \\ r_n &= Ds_n, \end{aligned} \quad (65)$$

and dynamical systems of the form

$$\begin{aligned} x_{n+1} &= g(x_n, x_{n-m}, u_n), \\ o_n &= o(x_n), \end{aligned} \quad (66)$$

for $n = 0, 1, \dots, N$. Here $u_n \in \mathbb{R}^{d_u}$ is the input, $o_n \in \mathbb{R}^{d_o}$ is the target output of the dynamical systems to be learned, $s_n \in \mathbb{R}^d$ is the hidden state of the learning model, $r_n \in \mathbb{R}^q$ is the model output, f is the tanh function applied component-wise, the maps g and o are Lipschitz continuous, and the matrices A, B, C, D and the vector b are learnable parameters. For simplicity, we take the initial functions to be $s_n = y_n = 0$ for $n = -m, -m + 1, \dots, 0$.

The following theorem shows that the delayed RNNs (65) are capable of approximating a large class of time-delay dynamical systems, of the form (66), to arbitrary accuracy.

Theorem 4. Assume that there exists a constant $R > 0$ such that $\max(\|x_{n+1}\|, \|u_n\|) < R$ for $n = 0, 1, \dots, N$. Then, for a given $\epsilon > 0$, there exists a delayed RNN of the form (65) such that the following holds for some d :

$$\|r_n - o_n\| \leq \epsilon, \quad (67)$$

for $n = 0, 1, \dots, N$.

Proof. The proof proceeds along the line of [54, 53], using the universal approximation theorem (UAT) for feedforward neural network maps and with straightforward modification to deal with the extra delay variables s_{n-n} and x_{n-m} here. The proof proceeds in a similar manner as the one provided in Section E.4 in [53]. The goal is to construct hidden states, output state, weight matrices and bias vectors such that an output of the delayed RNN approximates the dynamical system (66).

Let $\epsilon > \epsilon^* > 0$, $R^* > R \gg 1$ be parameters to be defined later. Then, using the UAT for continuous functions with neural networks with the tanh activation function [7], we can obtain the following statements. Given an ϵ^* , there exist weight matrices W_1, W_2, W_3, V_1 and a bias vector b_1 of appropriate dimensions such that the neural network defined by $\mathcal{N}_1(h, \tilde{h}, u) := W_3 \tanh(W_1 h + W_2 \tilde{h} + V_1 u + b_1)$ approximates the underlying function g as follows:

$$\max_{\max(\|h\|, \|\tilde{h}\|, \|u\|) < R^*} \|g(h, \tilde{h}, u) - \mathcal{N}_1(h, \tilde{h}, u)\| \leq \epsilon^*. \quad (68)$$

Now, we define the dynamical system:

$$p_n = W_3 \tanh(W_1 p_{n-1} + W_2 p_{n-m-1} + V_1 u_{n-1} + b_1), \quad (69)$$

with $p_i = 0$ for $i = -m, -m+1, \dots, 0$.

Then using the above approximation bound, we obtain, for $n = 1, \dots, N+1$,

$$\|x_n - p_n\| = \|g(x_{n-1}, x_{n-m-1}, u_{n-1}) - p_n\| \quad (70)$$

$$\leq \|g(x_{n-1}, x_{n-m-1}, u_{n-1}) - W_3 \tanh(W_1 p_{n-1} + W_2 p_{n-m-1} + V_1 u_{n-1} + b_1)\| \quad (71)$$

$$\leq \|g(x_{n-1}, x_{n-m-1}, u_{n-1}) - g(p_{n-1}, p_{n-m-1}, u_{n-1})\| \quad (72)$$

$$+ \|g(p_{n-1}, p_{n-m-1}, u_{n-1}) - W_3 \tanh(W_1 p_{n-1} + W_2 p_{n-m-1} + V_1 u_{n-1} + b_1)\| \quad (73)$$

$$\leq Lip(g)(\|x_{n-1} - p_{n-1}\| + \|x_{n-m-1} - p_{n-m-1}\|) + \epsilon^*,$$

where $Lip(g)$ is the Lipschitz constant of g on the compact set $\{(h, \tilde{h}, u) : \|h\|, \|\tilde{h}\|, \|u\| < R^*\}$.

Iterating the above inequality over n leads to:

$$\|x_n - p_n\| \leq \epsilon^* C_1(n, m, Lip(g)), \quad (74)$$

for some constant $C_1 > 0$ that is dependent on $n, m, Lip(g)$.

Using the Lipschitz continuity of the output function o , we obtain:

$$\|o_n - o(p_n)\| \leq \epsilon^* C_2(n, m, Lip(g), Lip(o)), \quad (75)$$

for some constant C_2 that is dependent on $n, m, Lip(g), Lip(o)$, where $Lip(o)$ is the Lipschitz constant of o on the compact set $\{h : \|h\| < R^*\}$.

Next we use the UAT for neural networks again to obtain the following approximation result. Given an $\bar{\epsilon}$, there exists weight matrices W_4, W_5 and bias vector b_2 of appropriate dimensions such that the tanh neural network, $\mathcal{N}_2(h) := W_5 \tanh(W_4 h + b_2)$ approximates the underlying output function o as:

$$\max_{\|h\| < R^*} \|o(h) - \mathcal{N}_2(h)\| \leq \bar{\epsilon}. \quad (76)$$

Defining $\bar{o}_n = W_5 \tanh(W_4 p_n + b_2)$, we obtain, using the above approximation bound and the inequality (75):

$$\|o_n - \bar{o}_n\| = \|o_n - o(p_n)\| + \|o(p_n) - \bar{o}_n\| \leq \epsilon^* C_2(n, m, Lip(g), Lip(o)) + \bar{\epsilon}. \quad (77)$$

Now, let us denote:

$$\tilde{p}_n = \tanh(W_1 p_{n-1} + W_2 p_{n-m-1} + V_1 u_{n-1} + b_1), \quad (78)$$

so that $p_n = W_3 \tilde{p}_n$. With this notation, we have:

$$\bar{o}_n = W_5 \tanh(W_4 W_3 \tanh(W_1 W_3 \tilde{p}_{n-1} + W_2 W_3 \tilde{p}_{n-m-1} + V_1 u_{n-1} + b_1) + b_2). \quad (79)$$

Since the function $R(y) = W_5 \tanh(W_4 W_3 \tanh(W_1 W_3 y + W_2 W_3 \tilde{p}_{n-m-1} + V_1 u_{n-1} + b_1) + b_2)$ is Lipschitz continuous in y , we can apply the UAT again to obtain: for any $\tilde{\epsilon}$, there exists weight matrices W_6, W_7 and bias vector b_3 of appropriate dimensions such that

$$\max_{\|y\| < R^*} \|R(y) - W_7 \tanh(W_6 y + b_3)\| \leq \tilde{\epsilon}. \quad (80)$$

Denoting $\tilde{o}_n := W_7 \tanh(W_6 p_{n-1} + b_3)$ and using the above approximation bound, we obtain $\|\bar{o}_n - \tilde{o}_n\| \leq \tilde{\epsilon}$.

Finally, we collect all the ingredients above to construct a delayed RNN that can approximate the dynamical system (66). To this end, we define the hidden states (in an enlarged state space): $s_n := (\tilde{p}_n, \hat{p}_n)$, with \tilde{p}_n, \hat{p}_n sharing the same dimension. These hidden states evolve according to the dynamical system:

$$s_n = \tanh \left(\begin{bmatrix} W_1 W_3 & 0 \\ W_6 W_3 & 0 \end{bmatrix} s_{n-1} + \begin{bmatrix} W_2 W_3 & 0 \\ 0 & 0 \end{bmatrix} s_{n-m-1} + \begin{bmatrix} V_1 u_{n-1} \\ 0 \end{bmatrix} + \begin{bmatrix} b_1 \\ 0 \end{bmatrix} \right). \quad (81)$$

Defining the output state as $r_n := [0, W_7] s_n$, with the s_n satisfying the above system, we arrive at a delayed RNN that approximates the dynamical system (66). In fact, we can verify that $r_n = \bar{o}_n$. Setting $\bar{\epsilon} < \epsilon/2$ and $\epsilon^* < \epsilon/(2C_2(n, m, Lip(g), Lip(o)))$ give us the bound (67) in the theorem. \square

F Additional Details and Experiments

In this section, we provide additional empirical results and details to demonstrate the advantages of τ -GRU when compared to other RNN architectures.

F.1 Speech Recognition: Google 12

Here, we consider the Google Speech Commands data set V2 [61] to demonstrate the performance of our model for speech recognition. The aim of this task is to learn a model that can classify a short audio sequence, which is sampled at a rate of 16 kHz from 1 second utterances of 2, 618 speakers. We consider the Google 12-label task (Google12) which is composed of 10 keyword classes, and in addition one class that corresponds to ‘silence’, and a class corresponding to ‘unknown’ keywords. We adopt the standard train/validation/test set split for evaluating our model, and we use dropout, applied to the inputs, with rate 0.03 to reduce overfitting.

Table 6 presents the results for our τ -GRU and a number of competitive RNN architectures. We adopt the results for the competitive RNNs from [53]. Our proposed τ -GRU shows the best performance on this task, i.e., τ -GRU is able to outperform gated and continuous-time RNNs on this task that requires an expressive recurrent unit.

Table 6: Results for Google12. Results indicated by * are produced by us, results indicated by + are from [53].

Model	Test Accuracy (%)	# units	# param
tanh RNN [53] ⁺	73.4	128	27k
LSTM [53] ⁺	94.9	128	107k
GRU [53] ⁺	95.2	128	80k
AsymRNN [11] ⁺	90.2	128	20k
expRNN [39] ⁺	92.3	128	19k
coRNN [52] ⁺	94.7	128	44k
Fast GRNN [33] ⁺	94.8	128	27k
LEM [53]	95.7	128	107k
Lipschitz RNN [15] [*]	95.6	128	34k
Noisy RNN [41] [*]	95.7	128	34k
iRNN [27] [*]	95.1	-	8.5k
TARNN [26] [*]	95.9	128	107k
ours	96.2	128	107k

F.2 Learning the Dynamics of Mackey-Glass System

Here, we consider the task of learning the Mackey-Glass equation, originally introduced in [45] to model the variation in the relative quantity of mature cells in the blood:

$$\dot{x} = a \frac{x(t-\delta)}{1+x^n(t-\delta)} - bx(t), \quad t \geq \delta, \quad (82)$$

where $\delta \geq 17$, $a, b, n > 0$, with x satisfying $\dot{x} = ax(0)/(1+x(0)^n) - bx$ for $t \in [0, \delta]$. It is a scalar equation with chaotic dynamics, with infinite-dimensional state space. Increasing the value of δ increases the dimension of the attractor.

For data generation, we choose $a = 0.2$, $b = 0.1$, $n = 10$, $\delta = 17$, $x(0) \sim \text{Unif}(0, 1)$, and use the classical Runge-Kutta method (RK4) to integrate the system numerically from $t = 0$ to $t = 1000$ with a step-size of 0.25. The training and testing samples are the time series (of length 2000) generated by the RK4 scheme on the interval $[500, 1000]$ for different realizations of $x(0)$. Figure 7 shows a realization of the trajectory produced by the Mackey-Glass system (and also the DDE based ENSO system considered in the main text).

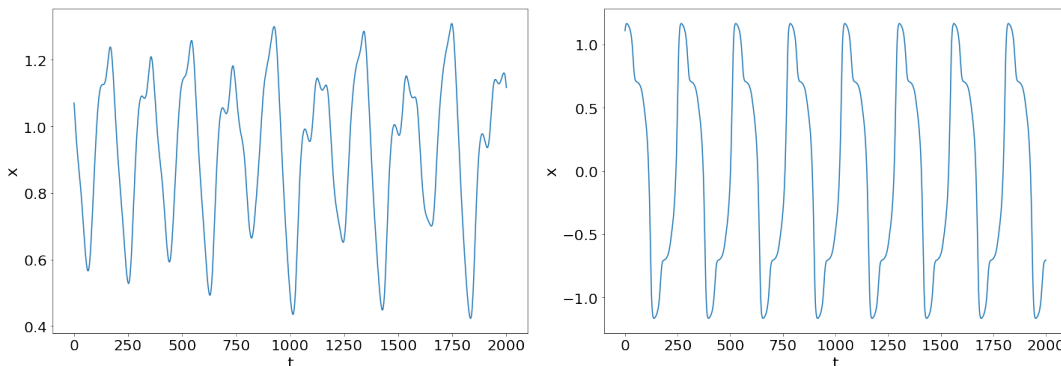


Figure 7: A realization of the Mackey-Glass dynamics (left) and the DDE based ENSO dynamics (right).

Table 8 shows that our τ -GRU model (with $\alpha = \beta = 1$ and using $\tau = 10$) is more effective in learning the Mackey-Glass system when compared to other RNN architectures. We also see that the predictive performance deteriorates without making full use of the combination of the standard recurrent unit and delay recurrent unit (setting either α or β to zero). Moreover, τ -GRU demonstrates improved performance when compared to the simple delay GRU model (Eq. (12)) and the counterpart model without using the gating. Similar observation also holds for the ENSO prediction task; see Table 7.

Figure 8 shows that our model converges much faster than other RNN models during training. In particular, our model is able to achieve both lower training and testing error (as measured by the root mean square error (RMSE)) with fewer epochs, demonstrating the effectiveness of the delay mechanism in improving the performance on the problem of long-term dependencies. This is consistent with our analysis on how the gradient information is propagated through the delay buffers in the network (see Proposition 1), suggesting that the delay buffers can propagate gradient more efficiently. Similar behavior is also observed for the ENSO task; see Figure 9.

Table 7: Additional results for the ENSO model prediction.

Model	MSE ($\times 10^{-2}$)	# units	# parameters
simple delay GRU (Eq. (12))	0.2317	16	0.897k
ablation (no gating)	0.4289	16	0.929k
τ-GRU (ours)	0.17	16	1.2k

Table 8: Results for the Mackey-Glass system prediction.

Model	MSE ($\times 10^{-2}$)	# units	# parameters
Vanilla RNN	0.3903	16	0.321k
LSTM	0.6679	16	1.233k
GRU	0.4351	16	0.929k
Lipschitz RNN	8.9718	16	0.561k
coRNN	1.6835	16	0.561k
LEM	0.1430	16	1.233k
simple delay GRU (Eq. (12))	0.2772	16	0.897k
ablation (no gating)	0.2765	16	0.929k
ablation ($\alpha = 0$)	0.1553	16	0.625k
ablation ($\beta = 0$)	0.2976	16	0.929k
τ-GRU (ours)	0.1358	16	1.233k

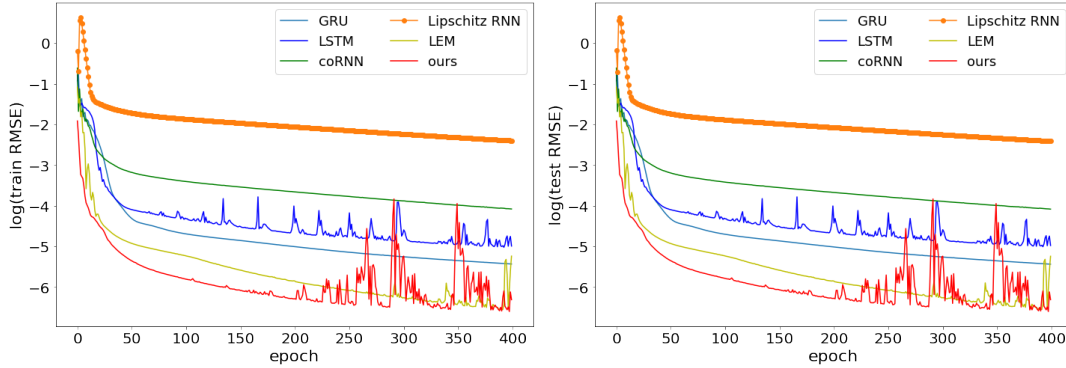


Figure 8: Train RMSE (left) and test RMSE (right) vs. epoch for the Mackey-Glass learning task.

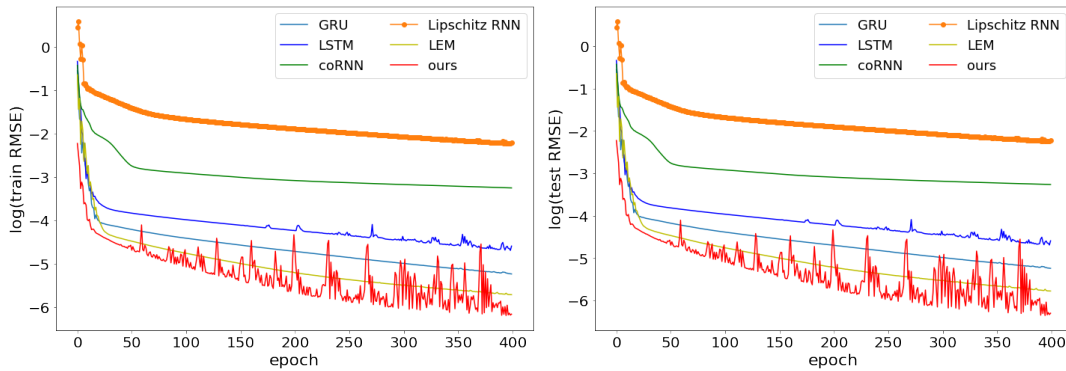


Figure 9: Train RMSE (left) and test RMSE (right) vs. epoch for the ENSO learning task.

G Tuning Parameters

To tune our τ -GRU, we use a non-exhaustive random search within the following plausible ranges for $\tau = 5, \dots, 200$. We used Adam as our optimization algorithm for all of the experiments. For the synthetic data sets generated by the ENSO and Mackey-Glass system, we used learning rate of 0.01. For the other experiments we considered learning rates between 0.01 and 0.0005. We used dropout for the IMDB and Google12 task to avoid overfitting.

Table 9 is listing the tuning parameters for the different tasks that we considered in this work.

Table 9: Summary of tuning parameters.

Name	d	lr	τ	dropout	epochs
Adding Task $N = 2000$	128	0.0026	900	-	200
Adding Task $N = 5000$	128	0.002	2000	-	200
IMDB	128	0.0012	1	0.04	30
HAR-2	128	0.00153	10	-	100
sMNIST	128	0.0018	50	-	60
psMNIST	128	0.0055	65	-	80
sCIFAR	128	0.0035	30	-	50
nCIFAR	128	0.0022	965	-	50
Google12	128	0.00089	5	0.03	60
ENSO	16	0.01	20	-	400
Mackey-Glass system	16	0.01	10	-	400

Sensitivity to Random Initialization. We evaluate our models for each tasks using 8 seeds. The maximum, minimum, average values, and standard deviations obtained for each task are tabulated in Table 10.

Table 10: Sensitivity to random initialization evaluated over 8 runs with different seeds.

Task	Maximum	Minimum	Average	standard dev.	d
IMDB	88.7	86.2	87.9	0.82	128
HAR-2	97.4	96.6	96.9	0.41	128
sMNIST	99.4	99.1	99.3	0.08	128
psMNIST	97.2	96.0	96.8	0.39	128
sCIFAR	74.9	72.65	73.54	0.90	128
nCIFAR	62.7	61.7	62.3	0.32	128
Google12	96.2	95.7	95.9	0.17	128